

The Tumultuous Formation of the Hubble Sequence at $z > 1$ Examined with HST/WFC3 Observations of the Hubble Ultra Deep Field

C. J. Conselice^{1*}, A.F.L. Bluck^{1,2}, S. Ravindranath³, A. Mortlock¹, A. Koekemoer⁴, F. Buitrago¹, R. Grützbauch¹, S. J. Penny^{1,5}

¹University of Nottingham, School of Physics & Astronomy, Nottingham, NG7 2RD UK

²Gemini Observatory, Hilo Hawaii 96720, USA

³IUCAA, Pune University Campus, Pune 411007, Maharashtra, India

⁴Space Telescope Science Institute, Baltimore, MD USA 21218

⁵Endeavour Fellow, Swinburne University of Technology, Hawthorn, Victoria 3122, Australia

Accepted ; Received ; in original form

ABSTRACT

We examine in this paper a stellar mass selected sample of galaxies at $1 < z < 3$ within the Hubble Ultra Deep Field, utilising WFC3 imaging to study the rest-frame optical morphological distribution of galaxies at this epoch. We measure how apparent morphologies (disk, elliptical, peculiar) correlate with physical properties, such as quantitative structure and spectral-types. One primary result is that apparent morphology does not correlate strongly with stellar populations, nor with galaxy structure at this epoch, suggesting a chaotic formation history for Hubble types at $z > 1$. By using a locally defined definition of disk and elliptical galaxies based on structure and spectral-type, we find no true ellipticals at $z > 2$, and a fraction of $3.2 \pm 2.3\%$ at $1.5 < z < 2$. Local counterparts of disk galaxies are at a similar level of 7–10%, much lower than the 75% fraction at lower redshifts. We further compare WFC3 images with the rest-frame UV view of galaxies from ACS imaging, showing that galaxies imaged with ACS that appear peculiar often contain an ‘elliptical’ like morphology in WFC3. We show through several simulations that this larger fraction of elliptical-like galaxies is partially due to the courser PSF of WFC3, and that the ‘elliptical’ class very likely includes early-type disks. We also measure the merger history for our sample using CAS parameters, finding a redshift evolution increasing with redshift, and a peak merger fraction of $\sim 30\%$ at $z \sim 2$ for the most massive galaxies with $M_* > 10^{10} M_\odot$, consistent with previous results from ACS and NICMOS. We also compare our results to semi-analytical model results and find a relatively good agreement between our morphological break-down and the predictions. We finally argue that galaxies classified visually as peculiar, elliptical and as peculiar ellipticals, all have similar structural and stellar population properties, suggesting that these galaxies are in a similar formation mode, likely driven by major mergers.

Key words: Galaxies: Evolution, Formation, Structure, Morphology, Classification

1 INTRODUCTION

Explaining the origin of the Hubble sequence of galaxies has remained one of the most outstanding problems in extragalactic astronomy. Massive galaxies in the nearby universe are largely in the form of ellipticals and spirals. These galaxies tend to not be undergoing significant galaxy or star for-

mation processes, and are the end result of evolution and formation over the past ~ 13.7 Gyr. However, deep Hubble Space Telescope (HST) imaging using both optical and near-infrared (NIR) cameras, such as ACS and NICMOS, have shown convincingly that the galaxy population at higher redshifts, particularly at $z > 2$, is dominated by irregular and peculiar galaxies that often have no obvious similarity, in terms of structure, to lower redshift galaxies (e.g., Driver et al. 1995; Abraham et al. 1996; Conselice et al. 2005, 2008;

* E-mail: conselice@nottingham.ac.uk

Lotz et al. 2004; Cassata et al. 2005, 2010; Overzier et al. 2010; Cameron et al. 2010). In fact the structures and morphologies of galaxies, and how they evolve, are now recognised as one of the most important methods for understanding galaxies, as it reveals not only the empirical evolution of a new parameter, but furthermore correlates with physical processes, such as merging, occurring within galaxies (e.g., Conselice 2003; Conselice et al. 2003b; Cassata et al. 2005; Grogin et al. 2005; Trujillo et al. 2007).

A major remaining issue in galaxy formation is solving the riddle of how the Hubble sequence came to be, and when this formation occurred. This problem of understanding the origin of the Hubble sequence can be defined most simply as uncovering when and how the disk and elliptical population in the nearby universe developed. This is a difficult problem since the population of disks and ellipticals is largely in place by $z \sim 1$ (Conselice et al. 2005) and to understand the formation of these systems one has to probe higher redshifts where the NIR is needed to resolve the location of most of the stellar mass in these galaxies.

There are however some existing clues for how this formation occurs from deep Hubble Space Telescope imaging, particularly from observations with the NICMOS camera (e.g., Conselice et al. 2005; Conselice et al. 2011). These observations show that, at rest-frame optical wavelengths, the types of galaxies seen changes gradually with time, such that disks and ellipticals are the dominate population at $z < 1$, while peculiars are the most common at $z > 2$ (Conselice et al. 2005, 2008). The population of ‘Hubble sequence’ galaxies roughly matches that of the peculiars sometime between $z = 1.5 - 2$, which is also the peak of the star formation rate in the universe (e.g., Bouwens et al. 2009).

There are at least two issues with these observations that still need to be addressed, and where HST Wide-Field Camera-3 (WFC3) observations will make a big impact in the next few years. One of these questions is understanding when the transformation between peculiar galaxies into disks and ellipticals occurs. The other major question is understanding the physical mechanisms responsible for driving the formation of these Hubble sequence galaxies. For example, are ellipticals and spirals formed through the accretion of gas, such as in cold streams (e.g., Dekel et al. 2009), and/or through in-situ formation of stars within an existing dark matter halo, and/or through mergers of existing galaxies (Hopkins et al. 2006)?

Recent observations of the kinematic structures of high redshift galaxies show that there is a large diversity of types, but with many star forming galaxies having a large velocity dispersion compared to their rotation (Genzel et al. 2006). This is either an indication that these systems are large disks collapsing, or that they are undergoing some type of merging activity (Shapiro et al. 2008). Overall, kinematic studies of $z > 2$ galaxies find that up to 1/3 of these systems have merger signatures in their kinematics, which is consistent with the fraction found from imaging (Conselice et al. 2003, 2008). However, these results are not entirely fool-proof, as other formation modes can mimic both the kinematic and morphological signatures. Furthermore the samples studied kinematically remain quite small, at a few 10s of systems. The relative role of these various assembly processes at high- z remain an open and important question

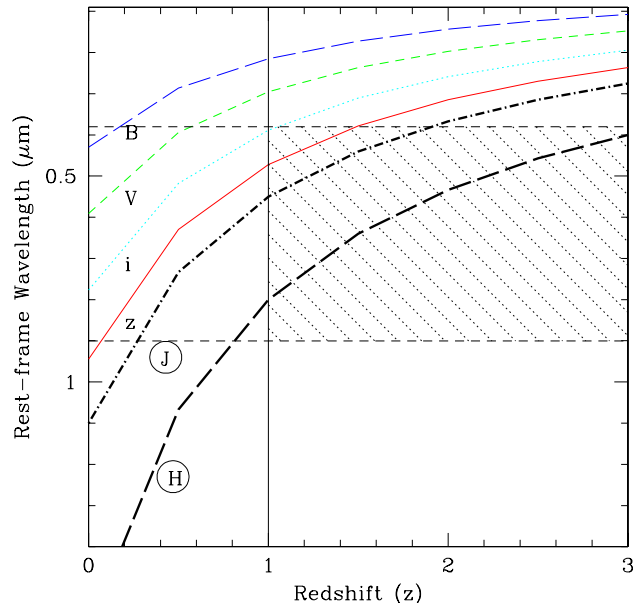


Figure 1. The rest-frame wavelength probed as a function of redshift for the two filters used in this study - J₁₁₀ and H₁₆₀ from WFC3 compared with the ACS filters of B₄₅₀, V₆₀₆, i₇₇₅ and z₈₅₀. The vertical line at $z = 1$ denotes the lower limit to redshifts considered in this paper. The shaded region shows the region where the rest-frame optical is probed, showing that for all but near $z \sim 1$ one must use NIR imaging to study the rest-frame structures of these galaxies.

regarding the mechanisms by which galaxy formation has occurred since $z \sim 3$.

New deep NIR observations of the high-redshift universe can provide some answers to these questions by examining the first question of when the Hubble sequence was in place, and to begin addressing the formation mechanisms for galaxies we see in today’s universe. Observations with the WFC3 of the Hubble Ultra Deep Field provides our first opportunity to go beyond NICMOS observations that currently exist. We describe a preliminary investigation of this problem using this early data and find that an apparently mostly smooth ‘early-type’ population appears to be the dominate one at high redshift, as compared with late-type or disk dominated galaxies. We further discuss the merger history and how it appears that high redshifts $1 < z < 3$ were not a particularly hospitable time for the formation of prominent late-type disks.

This paper is organised as follows. §2 gives an overview of the data and data sources we use, including previous work which we use to analyse our sample. §3 is a description of our structural measures, including CAS and Sérsic profiles fits, as well as our measures of the spectral types of our galaxies. §4 discusses our results, including morphological k -corrections, the types of galaxies found at high redshifts and a comparison to models, and how various classification methods compare with each other, while §5 is a summary

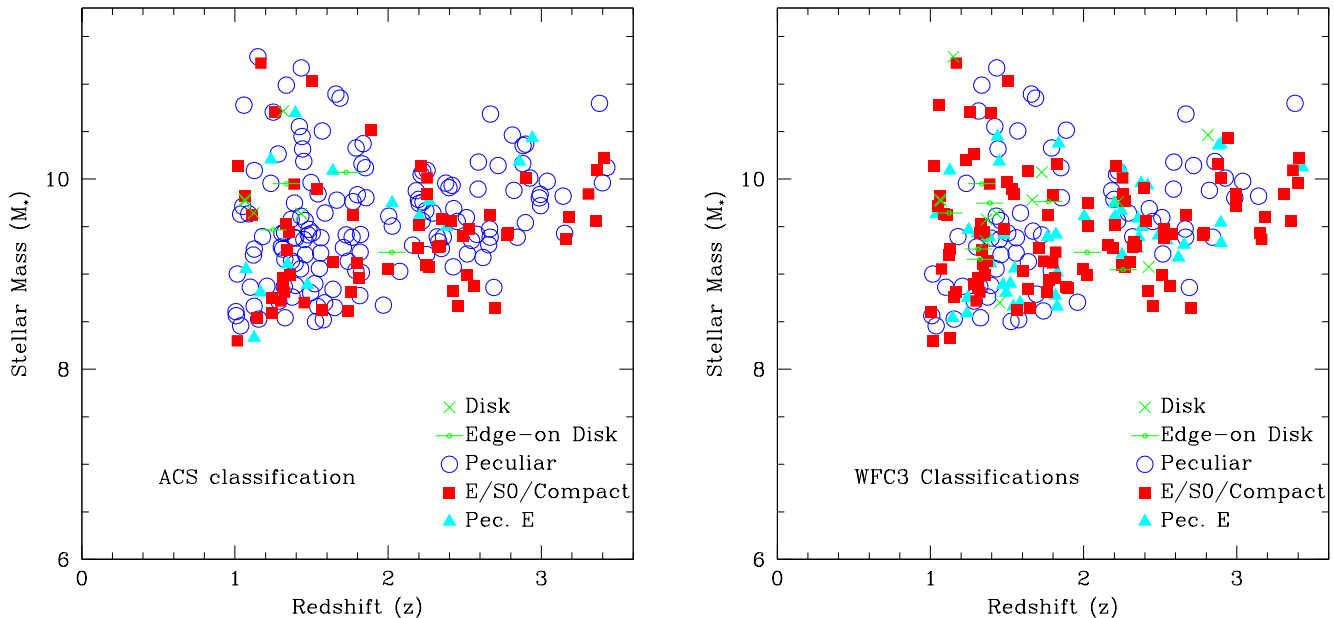


Figure 2. Stellar mass vs. redshift with the various galaxy types studied in this paper labelled. On the left we show the classifications for $z > 1$ galaxies carried out on ACS imaging of the UDF, and the right panel shows the classifications done using WFC3 at the rest-frame optical. The open blue circles are the galaxies classified visually as peculiars, the solid red boxes are ellipticals, S0s, and compacts, while the cyan triangles are ellipticals that appear to have a peculiarity. Disk galaxies are shown as green crosses for face on systems, with the edge-on systems displayed as a dot with a solid line.

of the results of this paper. We use a standard cosmology of $H_0 = 70 \text{ km s}^{-1} \text{ Mpc}^{-1}$, and $\Omega_m = 1 - \Omega_\Lambda = 0.3$ throughout.

2 DATA AND DATA SOURCES

The primary data used in this paper is the WFC3 observations of the Hubble Ultra Deep field located in the GOODS-South field (Giavalisco et al. 2004). We also use ACS and NICMOS imaging of the Hubble Ultra Deep Field (UDF) (Thompson et al. 2005; Beckwith et al. 2006) within this analysis, particularly when comparing with previous structural results (Conselice et al. 2008). The WFC3 field of view is 11 arcmin^2 , with a drizzled pixel scale of 0.03 arcsec per pixel, the same as for the ACS imaging. The filters we use in this study are the F160W (H_{160}) and the F110W (H_{110}) with a depth similar to the optical down to roughly $m_{AB} \sim 29$ using 16 orbits in the J-band and 28 orbits in H.

The UDF ACS images are taken within the F435W (B_{435}), F606W (V_{606}), F775W (i_{775}), and F850L (z_{815}) bands. The central wavelengths of these filters, and their full-width at half-maximum are: F435W (4297, 1038 Å), F606W (5907, 2342 Å), F775W (7764, 1528 Å), F850L (9445, 1229 Å). In Figure 1 we show the rest-frame wavelength probed by the WFC3 filters we use, as well as those for the ACS, demonstrating the necessity of using the near-IR to probe the rest-frame optical at $z > 1$ (shown as the dashed area).

The photometry and photometric redshifts we use are taken from our original study of the Hubble Ultra Deep Field (Conselice et al. 2008). The redshifts we use are pri-

marily from Coe et al. (2006) who measure the photometry of galaxies in the UDF within the BVizJH bands. The galaxies are detected with a modified version of SExtractor, called SExSeg. The photometry is PSF-corrected and aperture matched, removing the problem of matching magnitudes at different wavelengths due to variations in the PSF. This high fidelity photometry is then used to derive photometric redshifts, and for the stellar masses we measure for our galaxy sample.

The Coe et al. (2006) photometric redshifts are measured using the photometric redshift techniques from Benitez (2000), based on the optical and NIR photometry from ACS and NICMOS. In addition to these photometric redshifts we utilise 56 spectroscopic redshifts within the UDF field within our selection limits. All of the morphologies we determine in the near-infrared are examined with WFC3, and all the optical morphologies and structures with the ACS camera.

As this is a morphological, and not a photometric study, we must have more stringent constraints on which galaxies we can examine. We limit our study to systems which have magnitudes $z_{850} < 27$, such that we are not biased by low signal to noise imaging. This final ACS based catalogue of $z_{850} < 27$ sources contains 1052 unique galaxies within the ACS UDF field. Of these 299 are found within the smaller field of view WFC3 imaging of the UDF within the redshift range $1 < z < 3$. Note that although we use a z_{850} limit to define our sample, we later limit our analysis in the various analyses we carry out to a subsample of these. We do not include a discussion of lower or higher redshift galaxies in this paper. To run our morphological analysis requires

segmentation maps, and we ran SExtractor on the WFC3 imaging to obtain these maps which we later use within the morphological analysis (see Conselice et al. 2008).

3 STRUCTURAL MEASURES, STELLAR MASSES, AND SPECTRAL TYPES

In this paper we examine the morphological, structural and spectral properties of $z_{850} < 27$ galaxies in the UDF, as imaged in the WFC3 UDF pointing. We use an ACS z_{850} selection as this was done in our previous analyses of the UDF (Conselice et al. 2008). This allows us to compare directly how galaxy morphological and structural parameters vary with observed wavelength. We carry out several analyses of our WFC3 imaging using structural parameters, as well as stellar masses, and spectral types. We carry out these analysis in an independent way, thus lowering the effects of systematic errors on our overall results.

We carry out our visual and CAS analysis in several steps to maximise the usefulness of the data, and to minimise problems from contamination. We first create postage stamp images of each of our sample galaxies from our WFC3 mosaic. These are created by cutting out a $10'' \times 10''$ box of the UDF surrounding each galaxy, based on positions from the SExtractor catalog detections from Coe et al. (2006). Before this is done, the UDF WFC3 cutouts are cleaned of projected nearby galaxies and stars through the use of the ‘segmentation map’ produced by SExtractor (see Conselice et al. 2008). These segmentation maps are equivalent in size to the UDF image itself, with the difference being that it gives a numerical value for each pixel that reveals which galaxy it belongs to. These segmentation maps are used for photometry, but they are also useful for removing nearby galaxies. The procedure we use is to replace pixels of galaxies not being studied to the sky background with proper noise characteristics included. We then use these cleaned cutout images in our analysis.

After examining our sample visually, we found that occasionally features remained near galaxies, and had to be manually removed by hand. There were also cases where large late-type galaxies with spiral arms brighter than their centres tended to be picked up by the program more than once, and these were manually noted when spotted. In the following sections we describe our visual and quantitative analysis of these galaxy images within the UDF.

Likewise, we perform a parametric analysis on our data using the GALFIT package (Peng et al. 2002) to determine parametric sizes and Sérsic indices (§3.3). We use these Sérsic indices as another indicator of galaxy ‘type’ – i.e., what are likely progenitors of modern day disks and ellipticals. Furthermore, we also use the spectral energy distributions of our galaxies to determine their spectral types, which we explain in §3.4. By using spectral types we have a third and largely independent way to determine galaxy types, or their progenitors, at higher redshifts. In the case, instead of structure, we are examining their stellar populations – namely, early-type, disk, and starburst/Im.

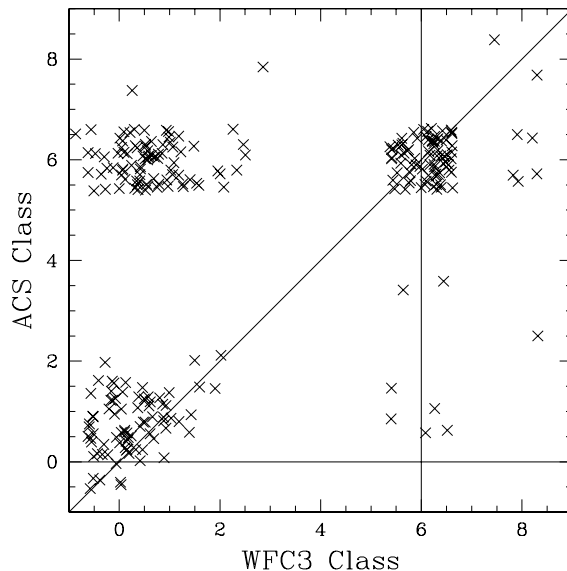


Figure 3. The relationship between the classification of the same galaxies within ACS and WFC3. The following key corresponds to the number schemes: 0 = Elliptical, 0.5 = peculiar elliptical, 1 = compact elliptical; 2 = early-disk, 3=late-disk, 6 = peculiar, 8 = edge-on disk galaxy. Note that the points on this plot are randomly offset to show the relative number at each position.

3.1 Visual Morphologies

We use several different methods in this paper to examine how the structures and morphologies of galaxies change with redshifts. First, one method involves a visual estimate of morphologies based on the appearance of our galaxies in the WFC3 imaging. The basic outline of how we carry out our classification process is given in Conselice et al. (2005a), Conselice et al. (2007b) and Conselice et al. (2008). The process is that we place each galaxy in the WFC3 imaging into one of nine categories: compact, elliptical, distorted elliptical, lenticular (S0), early-type disk, late-type disk, edge-on disk, merger/peculiar, and unknown/too-faint. These classifications are based only on how a galaxy looks, as seen in the observed H_{160} -band within WFC3. These galaxies are all resolved within at least 3-4 times the effective radius. We do not use information such as colour, size, redshift, etc to determine our classification types. Note that with WFC3, the resolution is not generally very high for these distant galaxies, and often galaxies look like ‘blobs’, and a classification type is sometimes more of an educated guess, and certainly prone to variation between classifiers. However, our classifications were done consistently, as described below. First we give the main types in which our classifications were done.

(i) Ellipticals : Ellipticals (Es) are centrally concentrated objects with no evidence for lower surface brightness, outer structures. We have 86 of these galaxies in our sample. In this paper, the meaning of ‘elliptical’ or ‘early-type’ henceforth is likely not the same as a pure elliptical selection at low redshift. Simulations (§4.3) show that what we classify

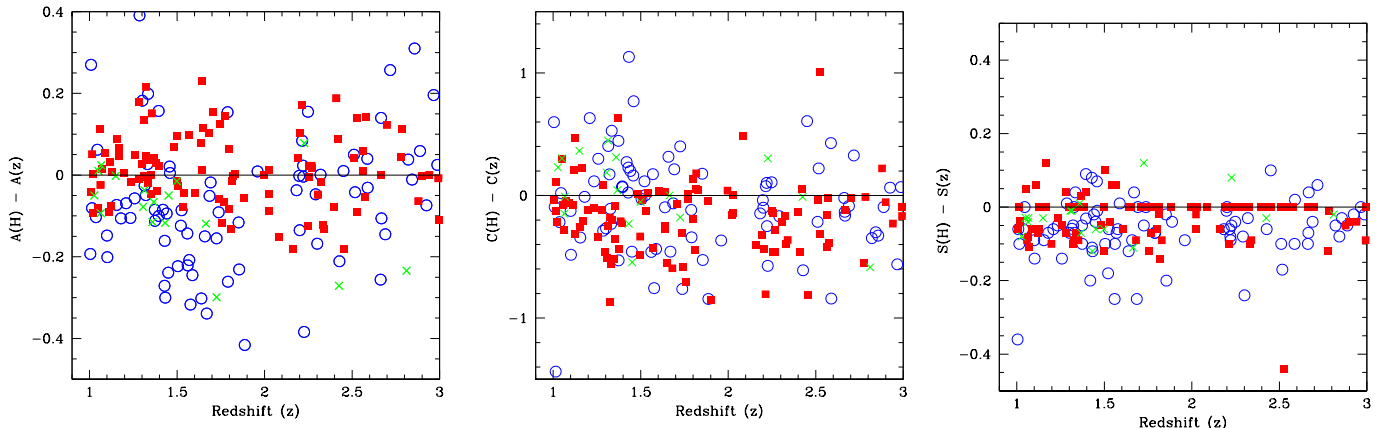


Figure 4. The change in the CAS parameters as a function of redshift. We trace in this figure the change between the observed $\sim 1.6 \mu\text{m}$ (H_{160}) and $\sim 0.9 \mu\text{m}$ (z_{850}) morphology. The symbol shape and colour denotes the galaxy type it denotes, as in Figure 2. The open blue circles are the galaxies classified visually as peculiars, the solid red squares are early-types, while the green crosses are disk galaxies. The horizontal line labels where there is no change between the measure structure in these two bands. Compared to morphological changes at $z < 1$ between rest-frame UV and optical, we find small changes at higher redshifts.

as ‘elliptical’ is likely a mixture of true ellipticals and spiral galaxies dominated by a bulge and/or mergers in a more relaxed phase.

(ii) Peculiar-Ellipticals : Peculiar ellipticals (Pec-Es) are galaxies that appear elliptical, but have some minor morphological peculiarity, such as offset isophotes, dual nuclei, or low-surface brightness asymmetries in their outer parts (58 systems). A full description of these galaxies is provided in Conselice et al. (2007).

(iii) S0s: S0s are galaxies that appear to have a smooth disk with a bulge. These galaxies do not appear to have much star formation, and are selected in the same way nearby S0s are. Our sample has only a single system making its contribution very small.

(iv) Compact - A galaxy is classified as compact if its structure is resolved, but still appears compact without any substructure. It is similar to the elliptical classification in that a system must appear very smooth and symmetric to be included. A compact galaxy differs from an elliptical in that it contains no features such as an extended light distribution or a light envelope. The fact that these systems are common at $z > 1$ while ellipticals are more commonly seen at lower redshifts suggests that they are potentially drawn from the same population. (28 systems)

(v) Early-type disks: If a galaxy contains a central concentration with some evidence for lower surface brightness outer light in the form of spiral arms or a disk, it is classified as an early-type disk. (14 systems)

(vi) Late-type disks: Late-type disks are galaxies that appear to have more outer low surface brightness disk light than inner concentrated light. (4 systems)

(vii) Edge-on disks: disk systems seen edge-on, and whose face-on morphology cannot be determined, but is presumably an S0 or spiral. (9 systems)

(viii) Peculiar/irregular: Peculiars and irregulars are systems that appear to be disturbed, or peculiar looking, including elongated/tailed sources. These galaxies are possibly in some phase of a merger (Conselice et al. 2003a), or are dominated by star formation (89 systems).

(ix) Unknown/too-faint: If a galaxy is too faint for any reliable classification it was placed in this category. Often these galaxies appear as smudges without any structure. These could be disks or ellipticals, but their extreme faintness precludes a reliable classification. We find that there are no systems in this category using our selection, although unclassifiable systems are found in the UDF ACS imaging.

Furthermore, we find that nine of our galaxies are not classifiable as they are unresolved, appearing as point sources. This may be misidentified stars, QSOs, or a mixture of these. They are not included in further discussions in this paper. Furthermore, we performed these same classifications on the ACS z_{850} -band imaging of the UDF, in the same manner as for the H_{160} imaging, for comparison purposes.

3.2 CAS Parameters

In addition to visual morphologies, we utilise the CAS (concentration, asymmetry, clumpiness) parameters to probe the structures of our galaxies quantitatively. The CAS parameters are a non-parametric method for measuring the forms of galaxies on resolved CCD images (e.g., Conselice et al. 2000a; Bershadsky et al. 2000; Conselice et al. 2002; Conselice 2003). The basic idea behind the CAS system (Conselice 2003) is that galaxies have light distributions revealing their past and present formation modes. This system can also be used to find specific galaxy types, as defined in the nearby universe, such as ellipticals and mergers/peculiars. For example, the selection $A > 0.35$ locates systems which are

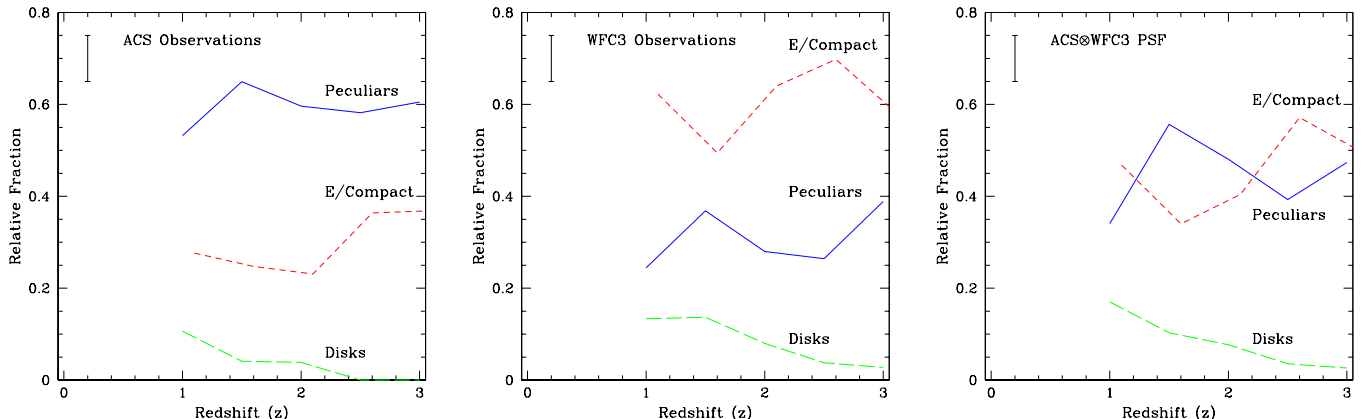


Figure 5. The relative distribution of galaxy types in the WFC3 Hubble Ultra Deep Field for systems selected with $z_{850} < 27$ as measured within three different images. The left panel shows the distribution of our classifications using the ACS imaging of the UDF (Conselice et al. 2008). The middle panel shows our new WFC3 UDF classifications and the right panel shows these same classifications done on a WFC3 image convolved with the ACS point spread function. Labelled on each panel are disks, ellipticals/S0s, compact galaxies, and peculiars. Note that the compact galaxies become an important population at higher redshifts.

nearly all major galaxy mergers in the nearby universe (e.g., Conselice et al. 2000b; Conselice 2003; Hernandez-Toledo et al. 2005; Conselice 2006b).

The basic procedure for measuring the CAS parameters is essentially the same as that presented in Conselice et al. (2008). First the galaxy is cut out from the main UDF WFC3 image from which the radii and the CAS parameters are measured. We measure the Petrosian radii for each galaxy from our images. This is the radius defined as the location where the surface brightness at a given radius is 20% of the surface brightness within that radius (e.g., Bershady et al. 2000; Conselice 2003). The exact Petrosian radius we use to measure our parameters is

$$R_{\text{Petr}} = 1.5 \times r(\eta = 0.2),$$

where $r(\eta = 0.2)$ is the radius where the surface brightness is 20% of the surface brightness within that radius.

We use circular apertures to measure our Petrosian radii and quantitative parameter estimation. We begin our estimates of the galaxy centre for the radius measurement at the centroid of the galaxy’s light distribution. Based on various test and simulations, we have found that the resulting radii do not depend critically on the exact centre, although for other parameters this can be more important (Conselice et al. 2000; Lotz et al. 2004). For more detail see Bershady et al. (2000), Conselice et al. (2000), Conselice (2003) and Conselice et al. (2008).

3.2.1 Asymmetry Parameter, A

The basic method for measuring the asymmetry is by taking an original galaxy image and rotating it 180 degrees about its centre, and then subtracting these two images (Conselice 1997). Important corrections are done for background light, and the radius has to be measured carefully, as explained in detail in Conselice et al. (2000a, 2002). Details such as how

centring is done is also described in Conselice et al. (2000a). The mathematical definition is

$$A = \min \left(\frac{\sum |I_0 - I_{180}|}{\sum |I_0|} \right) - \min \left(\frac{\sum |B_0 - B_{180}|}{\sum |I_0|} \right), \quad (1)$$

where I_0 is the original image pixels, I_{180} is the image after rotating by 180° . The background subtraction using light from a blank sky area, called B_0 , are critical for this process, and must be minimised in the same way as the original galaxy itself. Lower values of A imply that a galaxy is largely symmetric, which tends to be found in early type galaxies. Higher values of A indicate an asymmetric light distribution, which are usually found in spiral galaxies, or in the more extreme case, merger candidates.

3.2.2 Light Concentration C

The concentration index (C) is a measure of the intensity of light contained within a central region defined by a curve of growth radii, compared to a larger curve of growth radii. The exact definition is the log of the ratio of two circular radii which contain 20% and 80% (r_{20} , r_{80}) of the total galaxy flux,

$$C = 5 \times \log \left(\frac{r_{80}}{r_{20}} \right). \quad (2)$$

This index is sometimes called C_{28} . A higher value of C indicates that a larger amount of light in a galaxy is contained within a central region. Our measurement of the concentration correlates well with the mass and halo properties of galaxies (e.g., Bershady et al. 2000; Conselice 2003). Nearby galaxy values for the concentration index are $C = 2 - 3$ for disks, $C > 3.5$ for massive ellipticals, while peculiars span the entire range (Conselice 2003).

3.2.3 Clumpiness Parameter, S

The clumpiness (S) is a parameter for describing the fraction of light in a galaxy contained in clumpy light concentrations. Galaxies that appear ‘clumpy’, such as star forming systems, have a relatively large amount of light at high spatial frequencies, and high S indices. Smoother galaxies, such as ellipticals contain smaller S values. Clumpiness can be measured in a number of ways, the most common method used, as described in Conselice (2003) is,

$$S = 10 \times \left[\left(\frac{\Sigma(I_{x,y} - I_{x,y}^\sigma)}{\Sigma I_{x,y}} \right) - \left(\frac{\Sigma(B_{x,y} - B_{x,y}^\sigma)}{\Sigma I_{x,y}} \right) \right], \quad (3)$$

where, the original image $I_{x,y}$ is blurred to produce a secondary image, $I_{x,y}^\sigma$. This blurred image is then subtracted from the original image leaving a residual map, containing only high frequency structures in the galaxy (Conselice 2003). To quantify this, we normalise the summation of these residuals by the original galaxy’s total light, and subtract from this the residual amount of sky after smoothing and subtracting it in the same way. The size of the smoothing kernel σ is determined by the radius of the galaxy, and is $\sigma = 0.2 \cdot 1.5 \times r (\eta = 0.2)$ (Conselice 2003). Note that the centres of galaxies are removed when this procedure is carried out, typically the central 1/8th of the Petrosian radius.

3.3 Parametric Fitting – Sérsic Indices

While the non-parametric measures are one way to examine and quantify galaxy structure, utilising parametrised fits to light distributions of galaxies through an analytical form is another popular method for understanding the structural forms of galaxies. We fit to our WFC3 H₁₆₀-band imaging a single Sérsic profile of the form:

$$\Sigma(r) = \Sigma_e \exp(-\kappa[(r/r_e)^{1/n} - 1]) \quad (4)$$

We use the GALFIT package to fit equation (4) above to determine the Sérsic index (n) and the effective radius, (R_e). GALFIT was used to generate 2-D models of the light profiles of our sample galaxies using a single Sérsic function. The position, initial guess parameters for GALFIT (total mag, R_e , ellipticity, position angle, etc.) were taken from the SExtractor catalog. The background value is kept fixed at the value determined by SExtractor in the area around each galaxy. The constraints used when performing the fitting includes requiring that the centroid remains within 3 pixels of the input position, and the Sérsic index, n , does not exceed a value of $n = 10$. The PSF for convolving the analytical model was generated from the stars in UDF field using the PSF tasks in IRAF/DAOPHOT package, and then normalising these. When there are neighboring objects surrounding a specific object of interest, we perform simultaneous fits to the neighbours, which has been found to work better than masking the objects based on some isophotal threshold. In this paper we mostly make use of the Sérsic index, n , as a measure of the ‘disk-like’ or ‘elliptical-like’ nature of the galaxies within our sample. Typically galaxies with fitted $n > 2$ are elliptical like, and $n < 2$ are disk-like in a traditional interpretation compared with nearby galaxies (e.g., Trujillo et al. 2007; Buitrago et al. 2008). With GALFIT we also measure the axis ratio of each system, giving an ellipticity of $\epsilon = 1 - b/a$.

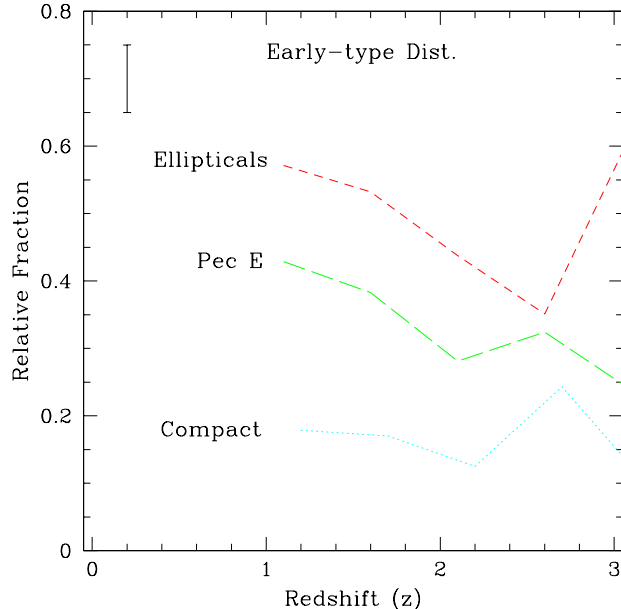


Figure 6. The distribution of galaxy types within the elliptical category in Figure 5 divided into normal ellipticals, compact ellipticals and peculiar ellipticals.

While it remains to be determined whether the kinematic interpretation of objects with rest-frame morphologies of a ‘disk’ and ‘spheroid’ nature match, the Sérsic index is a good rough guide to the overall shape of the light distribution within galaxies at different redshifts. These fits were also done using WFC3 data in Cassata et al. (2010) to investigate the size evolution of the most massive galaxies at $z < 3$, finding that they are indeed compact, as has been found in previous studies.

3.4 Spectral Types

Each galaxy in our sample has a morphological type which can be determined by the CAS parameters, by visual estimates of morphology, or by the measured Sérsic index. We furthermore utilise in this paper another method of determining galaxy types through the relative ages of their luminosity weighted stellar populations through fitting model spectra to observed spectral energy distributions (SEDs).

These observed spectral energy distributions are taken from the wealth of ancillary photometric data in the UDF field. In summary we use TFITed magnitudes, including the ACS optical, Spitzer IRAC data, U-band ground based photometry and deep IR photometry from ground-based telescopes. In detail these spectral types are based on imaging data from the VLT/VIMOS (U -band), HST/ACS imaging (F435W, F606W, F775W, and F850LP bands), VLT/ISAAC (J, H, and Ks bands), an Spitzer/IRAC bands at 3.6, 4.5, 5.8, and 8.0 μ m. The spectral types used in these

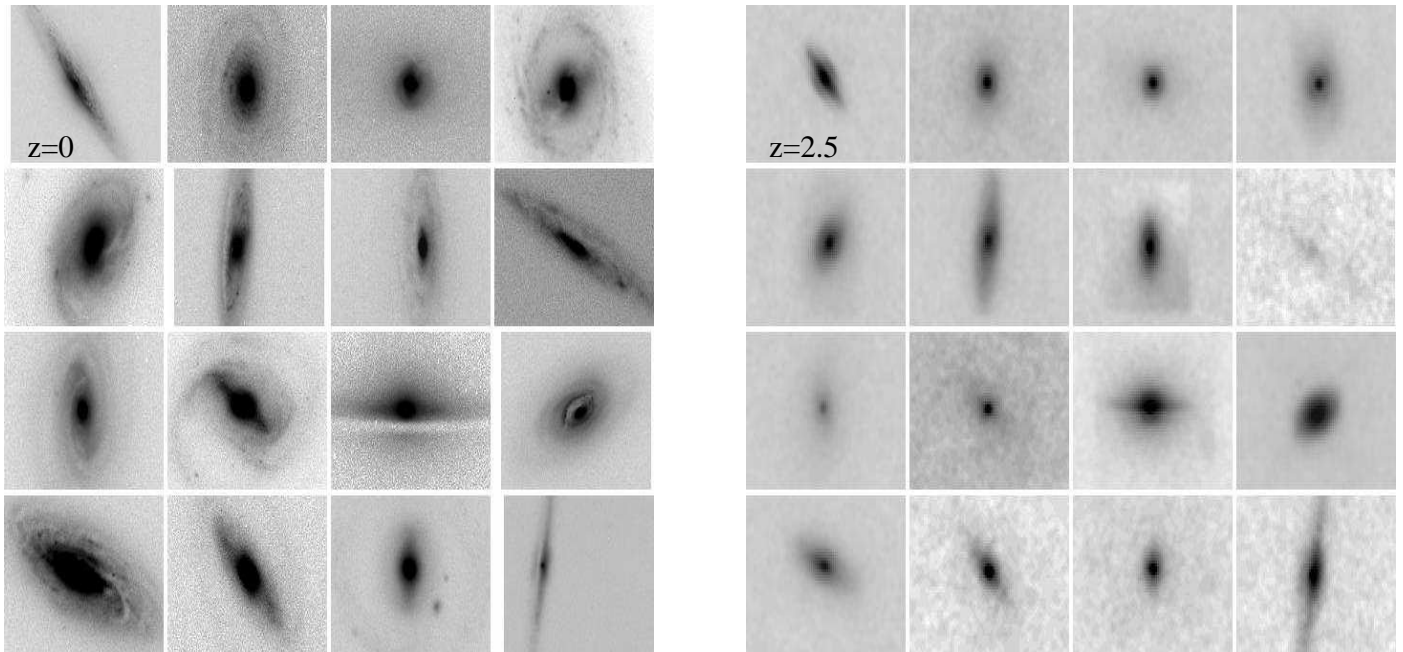


Figure 7. Example simulations of nearby galaxies which are originally observed at $z \sim 0$ imaged to how they would appear at $z = 2.5$ within the Hubble Ultra Deep Field F160W band as imaged with WFC3. These nearby galaxies are classified as early-type spirals (Sa and Sb). The typical sizes of these galaxies are several kpc in effective radii, and are at a variety of distances (see Conselice et al. 2000a). As can be seen, many of these systems would be difficult to classify as early-type disks, or even as galaxies which contain a disk in some cases.

fits include the SEDs based on the Coleman et al. (1980) types: E, Sbc, Scd, and Im based on spectra from nearby galaxies. In addition, starburst templates from Kinney et al. (1996) are included in these fits. We utilise the spectral types from these fits to compare with our morphological types. Further details of the fitting code, the templates used can be found in Dahlen et al. (2010).

4 RESULTS

In this section we analyse the morphological properties of our sample galaxies at $z > 1$. These galaxies constitute the brightest systems as seen in the Hubble Ultra Deep field and are amongst the most massive galaxies at high redshifts. We examine our sample in several ways. One is to simply look at the distribution of galaxy types at $z > 1$ which we have classified visually. The other is to examine how the morphologies of our systems differ between the WFC3 imaging and that seen in the ACS imaging of the same sample as examined in Conselice et al. (2008). We also examine how morphology, as judged visually, compares with spectral-type classifications from SEDs. Finally, we examine the structural parameters of our systems and compare what we calculate for the CAS values and Sérsic fits for our galaxies and the spectral-types and visual morphological estimates for these systems.

4.1 Morphological k -corrections

In Conselice et al. (2008) we investigate the morphological k -correction for galaxies seen in the UDF ACS field, particularly those at $z < 1$. We carried this out to determine how galaxies look different in a quantitative way at different wavelengths, and then used a quantitative version of this correction to put higher redshift galaxies at $z > 1$ at a pseudo rest-frame optical wavelength from which their merger fraction was derived (Conselice et al. 2008). In this paper, we are now able to derive what is the actual morphological k -correction between the H_{160} -band and the z_{850} -band for $z > 1$ systems, or rather how rest-frame optical and rest-frame ultraviolet morphologies differ.

First, to put this problem in context, the fundamental issue with using ACS data to examine the morphologies of $z > 1$ galaxies is shown in Figure 1 where the rest-frame wavelength probed by different ACS filters, and our WFC3 filters, are shown. This demonstrates that to probe the rest-frame optical light of galaxies at $z > 1.3$ we must use the observed infrared, and that the F160W (H_{160}) filter provides rest-frame optical coverage for galaxies between $1 < z < 3$. In the rest-frame optical, structural parameters such as the CAS parameters are largely similar (Taylor-Mager et al. 2007; Lanyon-Foster et al. 2011). Henceforth, later in this paper, we utilize mostly the H_{160} imaging to probe the morphologies and structures of our galaxy sample.

There are several ways to compare morphological k -corrections and how they evolve at $1 < z < 3$. One way to do this is to compare estimates of morphology in the ob-

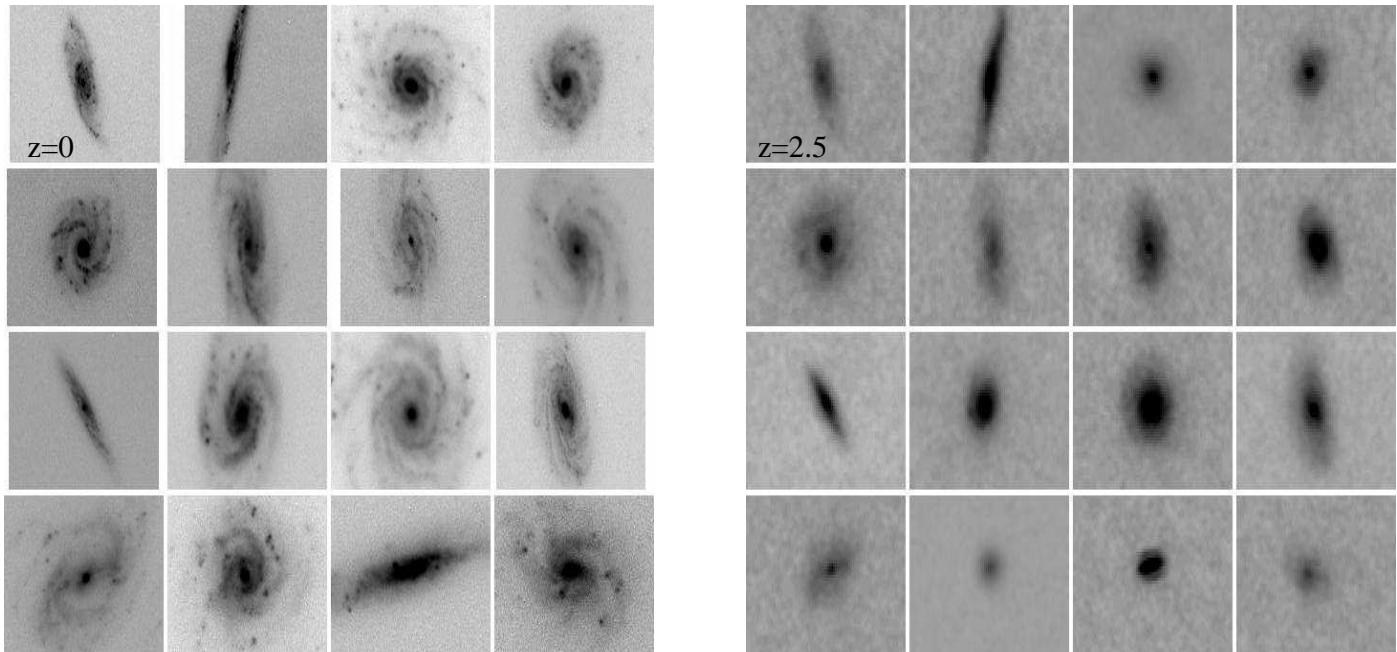


Figure 8. Example simulations of nearby galaxies which are originally observed at $z \sim 0$ imaged to how they would appear at $z = 2.5$ within the Hubble Ultra Deep Field F160W band as imaged with WFC3. These nearby galaxies are classified as late-type spirals (Sc and Sd). As can be seen, several systems are edge on in these simulations. The typical sizes of these galaxies are several kpc in effective radii, and are at a variety of distances (see Conselice et al. 2000a).

served z_{850} ACS band with the WFC3 H_{160} band. This comparison is shown in Figure 3. In general, galaxies along the 1:1 line have the same classification, and those which differ significantly, further away from this line, have increasingly different classifications in ACS and WFC3

A few outstanding deviations should be noted on Figure 3. The first is that for the peculiar class, as found in the ACS imaging, roughly half (78 out of 174) are also classified as peculiars in the WFC3 imaging. The remainder are disks (15 out of 174, or 9%), or early-types/compact galaxies (73 out of 174, or 42%). This implies that either roughly half of the peculiars seen at $1 < z < 3$ in the rest-frame UV are actually elliptical-like in the rest-frame optical, or that the larger PSF of the WFC3 imaging is creating galaxies that look smooth (see §4.2.1). We conclude that a significant fraction, but not all, of this change in type between wavelengths is due to the larger PSF of WFC3 compared with ACS §4.3.

Otherwise, for those galaxies classified as early-type in the ACS image, we find that almost all, or 75 out of 83 systems are also classified as an elliptical of some form in the WFC3 imaging. The remaining systems are mostly peculiars as seen by WFC3. The other slight difference in the classification between ACS and WFC3 is for systems classified as peculiar within the WFC3 imaging. For these systems, we find that 78 out of 89 systems (88%) are also classified as peculiar in the ACS imaging. The remainder are found to be early-types and two disks in the ACS imaging.

We furthermore investigate the quantitative morphological k -corrections for $z > 1$ galaxies by comparing how

the quantitative morphologies in the ACS z_{850} -band compares with the same morphologies in the H_{160} -band. Figure 4 shows the difference in the CAS parameters for our sample of galaxies from $z \sim 1 - 3$. What we find is generally similar to the trends seen for similar rest-frame wavelength morphological differences probed for $z < 1$ galaxies in Conselice et al. (2008) (see Table 1 and compare with Table 1 in Conselice et al. 2008). That is, the morphological k -correction, particularly for galaxies near $z \sim 1$ in the rest-frame optical and rest-frame UV are fairly similar to what is found at $z > 1$.

As expected galaxies are generally more asymmetric and clumpy when viewed at shorter wavelengths compared to the H_{160} -band, and surprisingly less concentrated for the ellipticals and peculiars. Table 1 lists the quantitative morphological k -correction for our galaxies between $z = 1$ and $z = 3$, using the same quantitative method as in Conselice et al. (2008). These values are the difference in the measured H_{160} morphology and the ACS z_{850} structural features.

We discuss below each of the CAS parameters and how their values differ between the H_{160} -band and the z_{850} -band. First, what we find from our measurements is that the concentration values are most different between the H_{160} and z_{850} bands for the ellipticals, in the sense that the ellipticals are more concentrated in the z_{850} -band than in the H_{160} -band. This is different from what is found for nearby galaxies (e.g., Taylor-Mager et al. 2007) where early

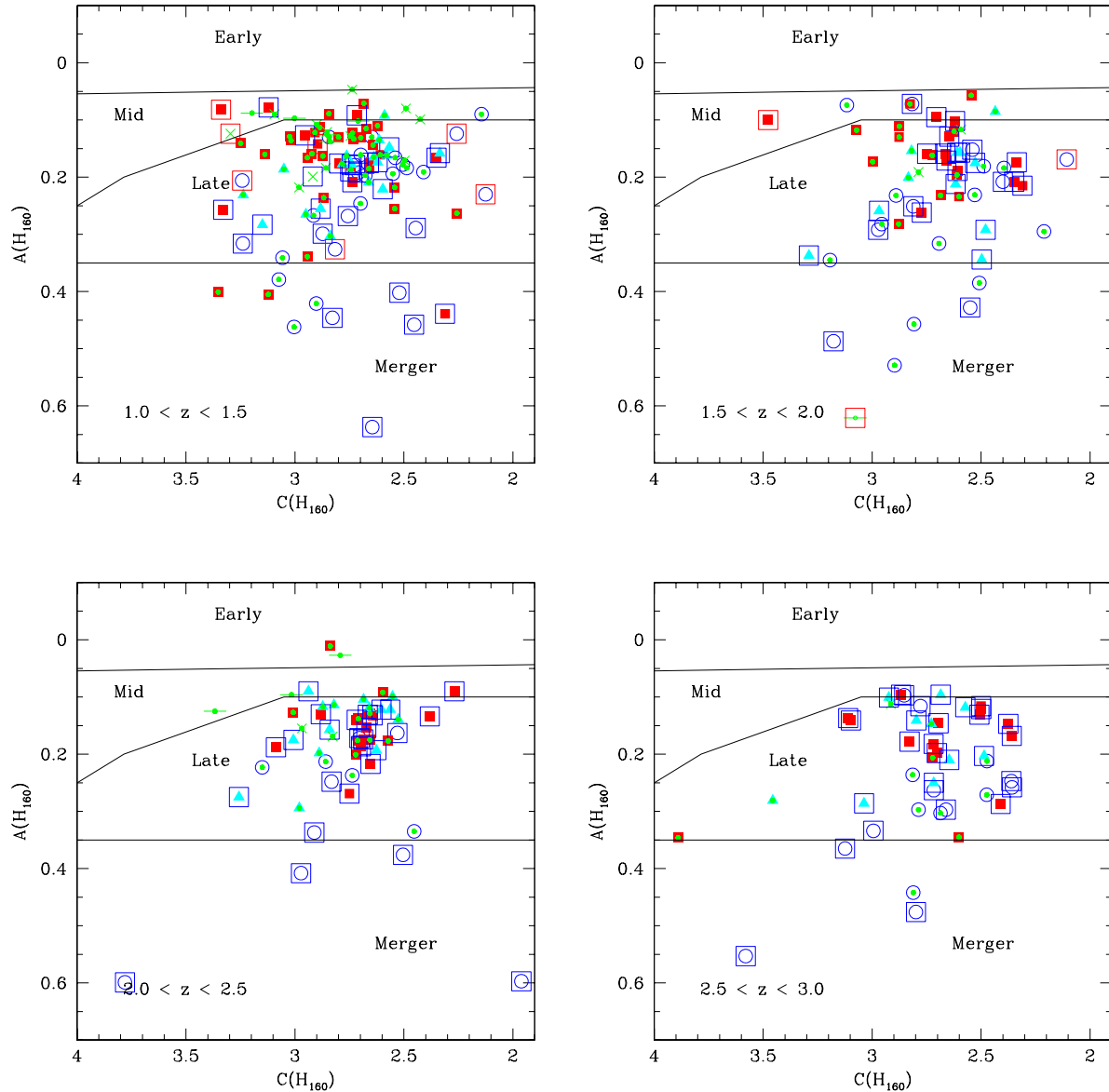


Figure 9. Plot showing the distribution of our WFC3 galaxy sample in the UDF as seen in the concentration-asymmetry plane of CAS space. The lines on each plot denote the region in which different galaxy types, as seen in the rest-frame optical are found in the nearby universe (e.g., Bershady et al. 2000; Conselice 2003). The redshift range for each panel is shown and goes from $1 < z < 3$. We show both the visual and spectral type classifications within this figure. The main visual symbol types for the points are the same as in Figure 1, such that the open blue circles are the peculiars, the red boxes are the early-types, the cyan triangles are the peculiar ellipticals, the green lines are edge-on disks and the green crosses are disks/spirals. We also show the spectral type classifications for the same galaxies in the following way: if the galaxy has a red open box surrounding it, it is classified as a early-type spectrally, open blue boxes are starforming systems, Im/starbursts, and those that have a green centre are classified spectrally as disk like or Sbc/Scd.

types become more concentrated at longer wavelengths. We also find this in the ACS UDF imaging at the lower redshifts ($z = 0.25 - 0.75$) where we find a positive value of $\Delta C/\Delta \lambda = 0.43 \pm 1.5$. However, we also find that early-type galaxies, as classified visually, are less concentrated in terms of their stellar mass distribution than in z_{850} -band light (Lanyon-Foster et al. 2011). This is likely due to central star formation dominating the morphologies of these systems, even if they are classified as early-type.

We also find that the peculiar galaxies within $z = 1 - 3$ have a similarly lower concentration as do ellipticals at longer wavelengths (Figure 2; Table 1). Spiral galaxies however, have a concentration difference near zero, and on average there is no morphological k -correction for these systems, likely due to the fact that these spirals are dominated by star forming regions that are easily visible in both the rest-frame UV and rest-frame optical.

In terms of the asymmetry parameter, we find a slight

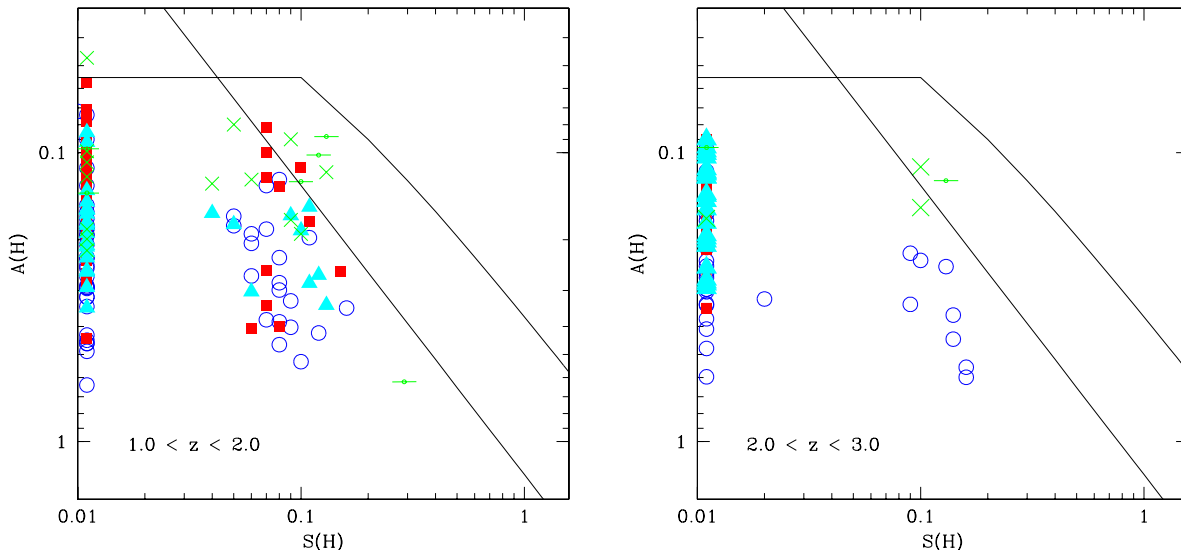


Figure 10. The relation between the asymmetry (A) and clumpiness (S) for our sample of WFC3 UDF galaxies in the H_{160} band. The solid line with the bend in it shows the relationship between these two parameters as found for nearby galaxies that are not involved in mergers (Conselice 2003). The straight line shows the relationship between these two parameters found at similar rest-frame wavelengths by Lanyon-Foster et al. (2011). This relationship is such that non-merging galaxies with a higher clumpiness has a slightly higher asymmetry, both due to star formation. Merging galaxies, where the structure is distorted due to bulk asymmetries from a merger have a larger asymmetry for their clumpiness. The point symbols are the same as in Figure 1 and the redshift range for each individual panel is listed. Note that galaxies which are generally more clumpy than asymmetric are classified as disk/spirals visually.

Table 1. The change in CAS parameters from the rest-frame optical to near-UV as function of redshift. These values are defined such that $\Delta = \lambda(H_{160}) - \lambda(z_{850})$

Peculiars	$z = 1 - 3$
$\frac{\Delta C}{\Delta \lambda} (\mu m^{-1})$	-0.59 ± 2.10
$\frac{\Delta A}{\Delta \lambda} (\mu m^{-1})$	-0.21 ± 0.68
$\frac{\Delta S}{\Delta \lambda} (\mu m^{-1})$	-0.24 ± 0.30
Ellipticals	$z = 1 - 3$
$\frac{\Delta C}{\Delta \lambda} (\mu m^{-1})$	-0.75 ± 1.30
$\frac{\Delta A}{\Delta \lambda} (\mu m^{-1})$	0.08 ± 0.54
$\frac{\Delta S}{\Delta \lambda} (\mu m^{-1})$	0.00 ± 1.19
Spirals	$z = 1 - 3$
$\frac{\Delta C}{\Delta \lambda} (\mu m^{-1})$	0.01 ± 1.20
$\frac{\Delta A}{\Delta \lambda} (\mu m^{-1})$	-0.34 ± 0.48
$\frac{\Delta S}{\Delta \lambda} (\mu m^{-1})$	-0.09 ± 0.23

change with respect to wavelength, which is less pronounced than what was found in Conselice et al. (2008) for systems at $z = 0.75 - 1.25$, comparing rest-frame $0.3 \mu m$ to $0.5 \mu m$. As would be expected, the peculiar galaxies and the spiral galaxies are more asymmetric on average in the z_{850} -band than in the H_{160} -band at $1 < z < 3$ (Table 1). However, we find that the elliptical galaxies are slightly more asymmetric in the H_{160} -band on average, although the difference is not large.

The clumpiness index has a similar pattern as the asymmetry index in that the peculiar and spiral galaxies have

on average higher clumpiness values in the z_{850} -band than in the H_{160} -band. The ellipticals have on average the same clumpiness, which is often zero, within the H_{160} -band and the z_{850} -band.

Overall, what we find is that at $z > 1$ there is less of a morphological k -correction than what is seen in the nearby universe, or at least at $z < 1$. This was originally noted in the lower resolution imaging of the Hubble Deep Field North when the NICMOS and WFC2 data were compared (e.g., Dickinson et al. 2000; Conselice et al. 2005). The meaning of this is fairly clear - the stellar populations that make up the light originating in the rest-frame optical is dominated by younger stars, or at least stellar populations that contain enough young stars to still be visible in the ultraviolet. This implies that we are not likely to learn much beyond our current understanding of this aspect of galaxy morphology in larger surveys such as CANDELS - however, this does lead to the possibility of utilising the morphological k -correction to find more evolved stellar population or ultra-dusty galaxies at these redshifts.

4.2 Galaxy Structure at $z > 1$

With WFC3 we are able to examine the rest-frame optical morphologies of galaxies at $z > 1$ in detail using the WFC3 J_{110} and H_{160} imaging. We use multiple approaches for this, including visual estimates of morphological types, as well as examining the CAS parameters and Sérsic fits to our galaxies.

The first observation we discuss is the distribution of galaxy visual structure with morphology and stellar mass, as shown in Figure 2. This Figure shows how our $z > 1$ sample

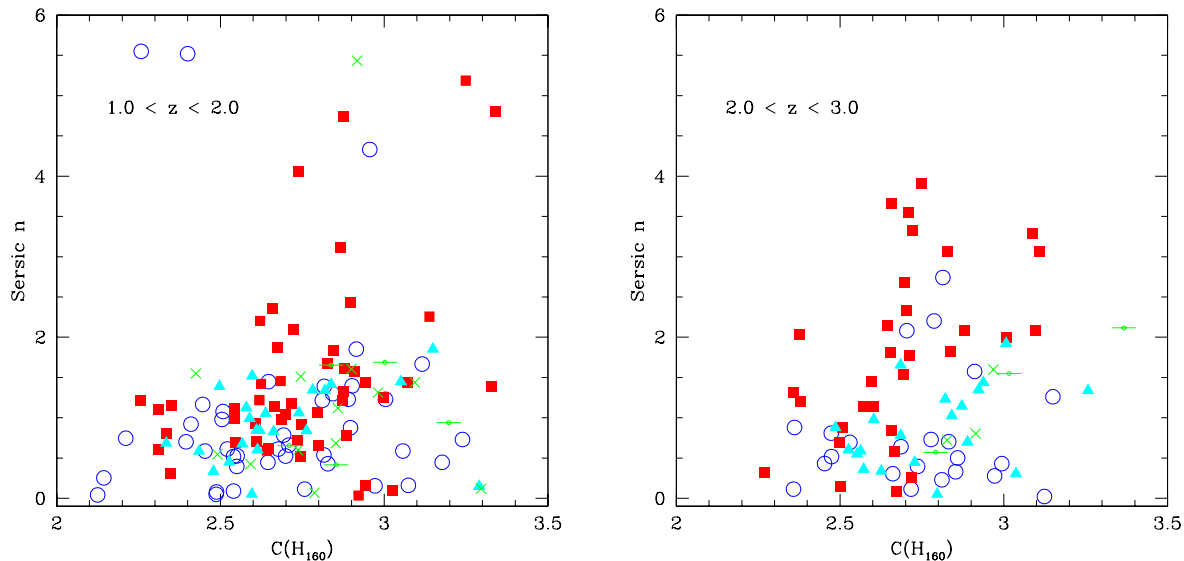


Figure 11. Plot showing the relationship between the concentration parameter C and the Sérsic index, n for galaxies divided into redshift ranges $1 < z < 2$ and $2 < z < 3$. Show on this panel as well are the visual classification types, as in Figure 1, such that the open blue circles are peculiars, the red boxes are the early-types, the cyan triangles are the peculiar ellipticals, the green lines are edge-on disks and the green crosses are disks/spirals.

is classified in both the ACS and WFC3 imaging of the UDF. The differences in these classifications can be visualised by comparing the two plots based on ACS and WFC3 imaging. A discussion of the visual apparent morphologies for these systems is included in Conselice et al. (2008).

Figure 2 shows that there is a broad distribution of types over the entire stellar mass and redshift range of our sample of galaxies. The most obvious difference between the ACS and the WFC3 classifications is that there are fewer peculiar galaxies in the WFC3 identifications than are seen in the ACS images. The peculiar systems seen in the ACS imaging mostly become peculiar ellipticals and E/S0/Compact systems when viewed in the rest-frame optical with WFC3, as discussed in §4.1.

We quantify this change by examining the distribution of morphological types as a function of redshift, as plotted in Figure 5. This shows the remarkable result that the peculiars which dominate the galaxy population within the ACS imaging, which probes the rest-frame UV at $z > 1$, drop by a factor of 1.5-2 in relative distribution at $z > 1$ when imaged within the WFC3 H₁₆₀-band. A large fraction of this change in types goes into the elliptical and compact populations. We do not see a large increase in the number of disk galaxies at high redshifts, however, we do see more of these systems in the WFC3 imaging (see §4.1).

We further plot the breakdown within the elliptical classification in Figure 6. Roughly half of the ‘elliptical’ population shown in Figure 5 is in the form of pure ellipticals, i.e., systems with no peculiarity. A further roughly 20% of the overall class of ‘ellipticals’ are compact and the remaining systems are peculiar ellipticals. There is no strong trend within the ‘elliptical’ class within these subtypes, although

the peculiar ellipticals do appear to increase slightly at lower redshifts.

If indeed the structures of the bulk of these galaxies are elliptical at high redshift this has important implications for galaxy formation studies. However, one major issue we have to deal with is the fact that the PSF of the WFC3 is larger than ACS and therefore it is important to quantify the effect of this larger WFC3 PSF on the classification of these galaxies. To address this we carry out several simulations to demonstrate that our results are robust. In §4.2.1 we convolve the PSF of WFC3 with the UDF ACS image and reclassifying the same galaxies. We also determine our classification biases through simulating lower redshift galaxies to how they would appear at higher redshift in §4.3.

4.3 Resolution and Depth Effect Biases

4.3.1 Effects of the WFC3 PSF

In all investigations of the structures and morphologies of distant galaxies a general problem is understanding how distant galaxies appear, and how they would look if we could image them as we do nearby galaxies. We address this issue in some detail in §4.3.2. Before examining this problem in depth, we first ask the simple question - is what we see in terms of the difference in structure between our galaxy images in the ACS and WFC3 due to the different PSFs, or a real effect?

The difference between the ACS and WFC3 imaging morphologies seen in §4.2 is not simply just a matter of wavelength differences, but also PSF and level of depth. In principle, any of these three can create morphological dif-

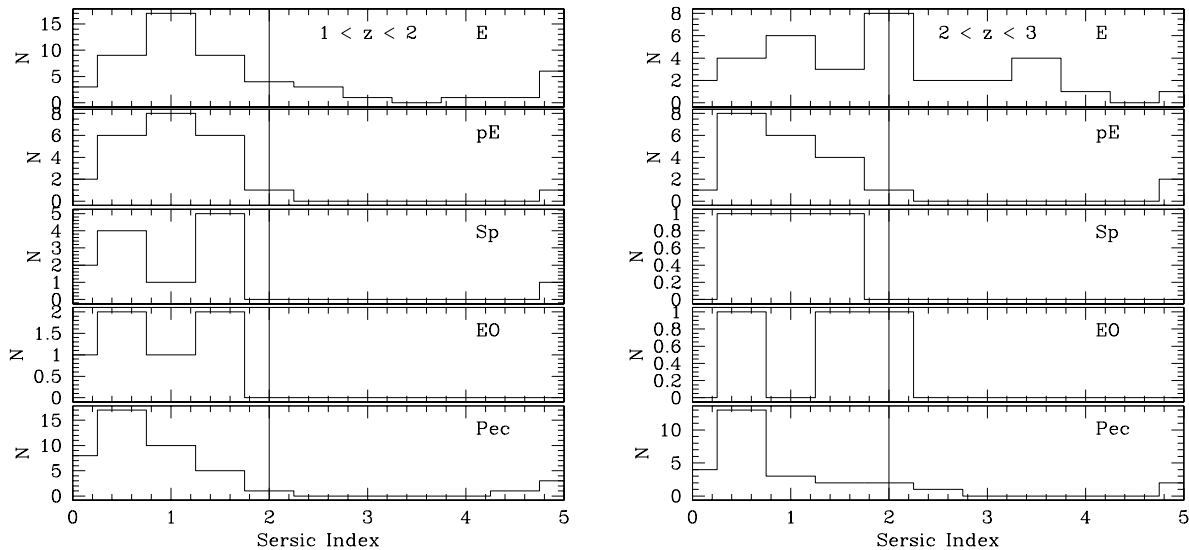


Figure 12. Figure showing the distribution of GALFIT Sérsic indices for our visually classified galaxies within the WFC3 UDF. Show are two panels divided by redshifts, with the left hand panel galaxies in our sample found at $1 < z < 2$, while the right panel shows galaxies at $2 < z < 3$. For each visually determined galaxy type: elliptical (E), peculiar elliptical (pE), spiral/disk (Sp), edge-on disk (EO) and peculiar (pec), we show the distribution of Sérsic indices. The vertical lines at $n = 2$ demonstrates the separation between galaxies that are ‘disk-like’ with $n < 2$ and those that are ‘elliptical-like’ with $n > 2$ (see Ravindranath et al. 2006; Buitrago et al. 2008).

ferences (Conselice et al. 2008), and while the first one due to wavelength is a ‘real’ (i.e., not instrument driven) effect, if there are differences due to PSF or depth, then this is simply due to the way the data was taken. To address this issue, we convolve the ACS image of the UDF in the z_{850} -band where our original work was carried out (Conselice et al. 2008) with the WFC3 PSF to determine how the morphologies of galaxies changes solely due to the slighter worse resolution of WFC3.

To carry this out we reclassify our galaxies seen in the new convolved image in the same way we did on the original ACS and WFC3 images (Figure 5). We carry out this classification in the same way we did our original classifications. This allows us to determine, and separate, the contribution to the change in morphology as resulting from different PSFs between the ACS and WFC3 camera as opposed to differences produced from probing different rest-frame wavelengths.

What we find is that the disk galaxy fraction is similar between the ACS, WFC3, and the ACS convolved with the WFC3 PSF image, classifications. However, there is clearly a difference between the fractions of peculiars and early-types when comparing the ACS WFC3 PSF convolved image with the WFC3 one. While we find a large fraction of E/Compact systems within the WFC3 images at all redshifts, we do not see the same results in the ACS WFC3 convolved image. In fact, while the number of early-type systems in the convolved ACS imaging increases from roughly a 30% fraction to about 45% after convolving with the WFC3 PSF. The peculiar fraction also drops from roughly 60% to 50%. This is significantly different from the WFC3 imaging classifications where ellipticals make up 60% of the population and peculiars are at $\sim 30\%$. This demonstration shows that over

half of our classifications in the WFC3 imaging are either due to identifying the correct galaxy type, or are due to morphological k -corrections.

4.3.2 Galaxy Structure Simulations

In the previous section we examine how galaxies in the UDF ACS image would appear after convolved with the WFC3 PSF. This approach is useful when comparing the WFC3 and ACS classifications, but they do not account entirely for the effects of redshift on the appearance of galaxies as they change through redshift. To account for this, we carry out a series of full simulations of taking galaxies at $z \sim 0$ to how they would appear at higher redshifts. Within this discussion, we use simulations of nearby galaxies placed at $z = 2.5$ as a fiducial amount of change for nearby galaxies to within the redshifts of this study ($1 < z < 3$).

These simulations are based on the method of simulating nearby galaxies at higher redshift as outlined in Conselice et al. (2003). Similar simulations have been carried out when examining morphologies in ACS imaging in Conselice (2003) and Conselice et al. (2008), and for NICMOS and WFC2 imaging in Conselice et al. (2003). These simulations are also used to determine how quantitative structural parameters change with redshift as outlined in Conselice et al. (2003, 2008).

These simulations are based on real images, taken in optical B-band, for nearby galaxies, using the sample from Frei et al. (1996). This sample is discussed in terms of morphology in Conselice et al. (2000a) and Bershady et al. (2000). Suffice it to say that this sample consists of bright nearby galaxies, mostly ellipticals and spirals. We do not consider merger simulations in this paper, although they have been

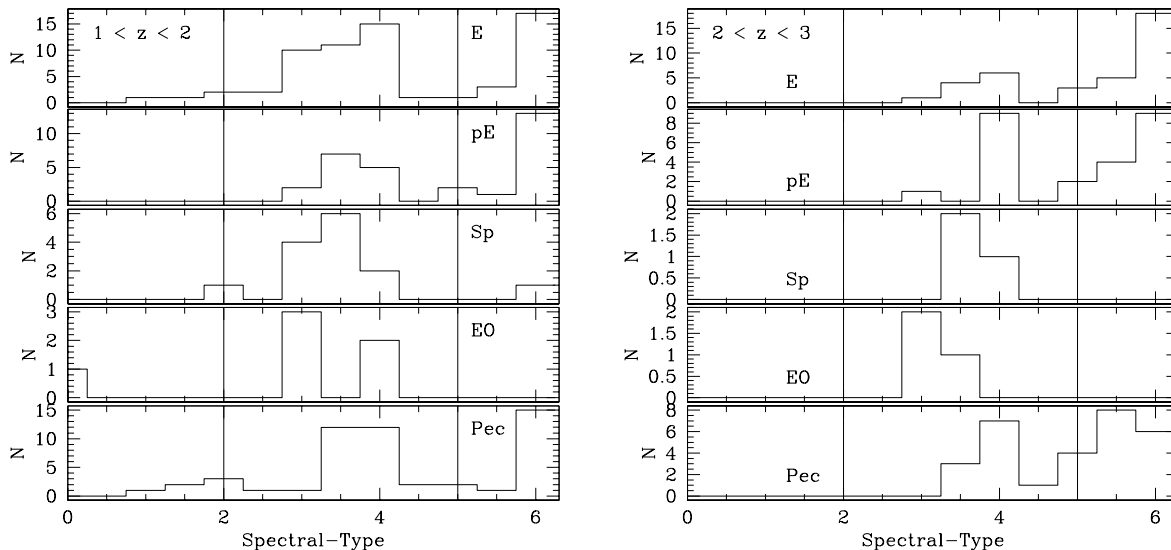


Figure 13. Figure showing the distribution of spectral types for our visually classified galaxies within the UDF. Show are two panels divided by redshifts, with the left hand panel galaxies in our sample found at $1 < z < 2$, while the right panel shows galaxies at $2 < z < 3$. For each visually determined galaxy type: elliptical (E), peculiar elliptical (pE), spiral/disk (Sp), edge-on disk (EO) and peculiar (pec), we show the distribution of spectral types for each. These types are such that: 1 = E, 2=Sbc, 3=Scd, 4=Im and 6=Starburst. The vertical lines show the division between early types at < 2 , mid-types or disk at $2 - 5$, and star forming galaxies, such as irregulars at > 5 .

discussed in detail in Conselice (2003), and will be the focus of future papers on this topic.

The simulations are done essentially by taking these nearby galaxies, as imaged with the Lowell 1.5 m telescope and placing them as they would appear in our WFC3 imaging of the UDF. All aspects of the Hubble Space Telescope, and the WFC3 imager, are considered in this simulation, including its: aperture, band width of different filters, throughput, pixel scale, read-noise, dark current, as well as using the empirically derived sky background (e.g., Giavalisco et al. 1996; Conselice 2003). Furthermore, we also experimented with two PSFs - one calculated from Tiny Tim and another based on stacking real stars from WFC3 imaging in other fields, such as the GOODS Early Release Observations.

The process in carrying out these simulations is outlined in detail in Conselice (2003) and we only give a summary of this here. The nearby galaxy image is first reduced in angular size to how it would appear at the simulated redshift. Next the flux is reduced by $(1+z)^4$ to account for surface brightness dimming. A background is then created which include all noise contributions, the major one being from the WFC3 background, which is at a level of $\sim 0.5 \text{ e}^{-} \text{ s}^{-1} \text{ pix}^{-1}$, which is around a factor of ten higher than for ACS. The galaxy is then placed into this simulated background, and the WFC3 PSF is applied to the image. We increase the surface brightness of each image by 1 magnitude, as it is known that distant galaxies are brighter than nearby galaxies by roughly this amount, with passive evolution with an exponentially declining star formation rate producing at least this much evolution.

Figure 7-8 shows examples of these simulations, for galaxies both before and after the simulation. We only show

in this paper the disk galaxies, as mergers and ellipticals nearly always are identifiable as such when simulated at higher redshift. We divide these disks in early-types (Sa through Sb; Figure 7) and late-types (Sc and Sd; Figure 8). The results are at times worrying for the simple reason that many of these galaxies would appear to be classified visually as ellipticals. In fact, the problem is more acute for the early type disks where the bulge component tends to dominate the appearance of the galaxy after it has been simulated. Viewing these galaxies as we did with *ds9* it would be difficult to always identify these as disks, especially as morphological classification is a subjective process, and different classifiers will classify the same galaxy in a different way.

In general for the late-type (Figure 8) and to a lesser extent the early-type disks (Figure 7) the simulated galaxies appear to have a morphology that is mostly bulge. However, these systems often have fainter outer ‘halo’-like material which can be interpreted, if identified correctly, as a disk system. However, it is possible that these systems could be identified as ellipticals with an outer envelope. In this paper, we were therefore careful to carry out our classifications of disks based on whether or not a roughly symmetrical outer portion of light was detected in an otherwise bulge system. Regardless, it is obvious that even with deep UDF WFC3 imaging that much of the structure in spiral galaxies is lost. Clearly spiral arms can no longer be identified, and often the disk itself is much less prominent than the bulge, undoubtedly this is due to the lower surface brightness of disks. This will be a major issue when interpreting shallower CANDELS data.

We classify our simulated sample as we did our original, and find that within these conditions we would have

misclassified 1/4th of the disk galaxies in the Frei samples as ‘early-types’. This is similar to the fraction of galaxies we misclassify in the ACS imaging due to the larger PSF. The reasons for these is likely similar, and due to the larger PSF of WFC3. We account for this in our analysis of the overall evolution of types in §4.4.

A major caveat to these simulations is that it is likely that disk galaxies in the early universe are potentially different from modern disks. We know that galaxies, even those with a disk-like morphologies and Sérsic indices indicating disks, are smaller by a factor of a few at $z \sim 2.5$ for at least the most massive systems (Buitrago et al. 2008). This will make it harder to identify disks if they are indeed smaller and therefore more difficult to resolve. On the other hand, we know that the quantitative morphological distribution for massive galaxies is quite different at these redshifts than today, and that any disks at these redshifts will likely not have as prominent bulges as contemporary disks. Furthermore, disks at high redshifts are potentially undergoing significant amounts of star formation, making their disks easier to identify and study. All of these features will have to be examined in more detail in future papers.

4.4 Overall Results of Apparent Morphological Evolution

In summary, the correction for PSF effects within WFC3 is at a level of 30-40% at most, as described in §4.3.1. This is verified by our analysis of simulations of nearby galaxies placed at high redshift (§4.3.2). In these simulations, we still find that ‘early-type’ morphologies are the dominate one at $1 < z < 3$. At most a correction would bring down the E/compact line in Figure 5 to roughly 40-50% – which is still much higher than what is implied with the ACS imaging, as well as different from previous results (Conselice et al. 2008). Therefore one major conclusion from this work is that high redshift galaxies appear to be more early-type than disk-like. However, this is only for our mass range, which is from roughly $\log M_* = 9$ to just above $\log M_* = 10$. This trend is potentially different for galaxies with $\log M_* > 11$ as seen in the GOODS NICMOS Survey (Buitrago, Trujillo & Conselice 2011).

However, as we show in the remainder of this paper, these galaxies, while appearing to be early-types are anything but analogs of early-type, in terms of their stellar populations, and they are likely undergoing significant evolution. Already, this can be seen by the fact that there is a morphological k -correction for WFC3 identified early-types, which appear as distorted systems in the rest-frame UV as probed by the ACS camera. We discuss the structures of these early-types as well as their spectral types, demonstrating the ongoing evolution of the Hubble sequence at $1 < z < 3$.

4.5 Quantitative Structure and Spectral Types

4.5.1 CAS and Sérsic Classifications

In Figure 9 we show the locations of our sample in concentration-asymmetry space and label our galaxies according to both their spectral and visual classification type. This plot is best understood by looking for boxes that agree,

or otherwise, in terms of the two colours plotted at each point. A blue box is for a starburst/Im spectral type, and a red box is for an E spectral type, while a green central dot is for Sbc/Scd spectral types. If the two colours are the same then the two ways of classifying that galaxy through visual and SED spectral-types are the same. If they differ then they do not agree.

The most remarkable feature of this diagram is that there is a significant amount of systems which are classified as having different spectral and morphological types throughout. What can be seen however, is that there is some relation between spectral galaxy type and position on the concentration-asymmetry plane. The starburst/Im classifications are nearly all in the higher asymmetry part of the distribution at $z < 2$. This however, changes at $z > 2$ where the starburst/Im types are found throughout the concentration/asymmetry plane. This is another indication that the quantitative measurements of structure at $z > 2$, particularly for lower asymmetry systems, cannot be interpreted in exactly the same way as a lower redshifts (e.g., Conselice et al. 2008).

Furthermore, as Figure 9 shows, there is not always a good agreement between visual estimates of morphology and their positions in the CA space. The disk galaxies, both those classified as such visually and through spectral energy fits to SEDs are often different objects. Furthermore the peculiar galaxies have a high asymmetry at each redshift, and often the peculiars are the majority of the systems in the merger region of CAS space, with $A > 0.35$. However, those galaxies classified visually as early-types are often found in the region of CA space occupied by the location of late-type galaxies in the nearby universe. This does not imply that these systems are late-types, but that they have asymmetry values that are larger, with around $\langle A \rangle \sim 0.2$. This is significantly higher than the average asymmetry for early types in the nearby universe which have values $\langle A \rangle = 0.02 \pm 0.02$, which is more than 10σ different from higher redshift galaxies. This clearly shows that the visually identified ellipticals are in a formation mode.

We furthermore show on Figure 10, the asymmetry-clumpiness plane of the CAS space. Many objects are too smoothed by the WFC3 PSF to measure this parameter (see Conselice 2003). However, those systems which are the most clumpy, as compared to their asymmetry, are the galaxies identified visually as disk systems. This is due to the fact that these visually identified disks are undergoing intense star formation in clumps, and potentially, using a comparison of asymmetry vs. clumpiness is a powerful way to identify these systems in WFC3 data.

We can get a further idea regarding the distribution of the properties of various high redshift Hubble types by examining the Sérsic fitted n index vs. the concentration parameter for our systems as labeled by spectral type. Figure 11 shows this, where we plot the spectral type as different symbols. In general, we find that galaxies with higher Sérsic indices have higher concentration values, with most systems at $n > 2$ having a concentration value $C > 2.7$, typically the value for early-types in local universe (Conselice 2003). However, clearly there is significant scatter in these values, and the galaxies identified visually as early-types (red boxes) are in every location of this diagram. The disk galaxy sys-

tems (the green crosses) however show that at least the disk galaxy systems are found at lower Sérsic indices of $n < 2$.

Figure 12 shows the distribution of the Sérsic indices for our sample, showing the range of values for each visually classified type, and that most visually classified ellipticals have lower Sérsic indices. This demonstrates that at least a fraction of the early-types, or the progenitors of early-types, have the expected Sérsic morphology, but still have enough residual star formation to have spectral types such as Sbc or starburst (Figure 13; §4.5.2). Figure 14 on the right hand side, furthermore shows that much of the $n > 2$ systems have a starburst spectral-type, and thus we may be seeing the epoch of the formation of the bulk of early types at $z > 2$ when finding bona-fide early types as a non-star forming, morphologically identifiable early-type, will be rare at these times (Bauer et al. 2011).

4.5.2 Spectral Type Classifications

When examining galaxies and classifying them into different types, there are several ways to proceed. The traditional way is to examine systems in optical light and to classify the galaxy onto the Hubble sequence or a variation of the Hubble sequence. For nearby galaxies there is a good correlation between the Hubble type and physical parameters of the galaxy, such as the colour, star formation history, size, etc. (e.g., Roberts & Haynes 1994; Conselice 2006a). However, this relationship may not hold at higher redshifts. Therefore, it is desirable to classify galaxies into spectral types, as well as visual estimates of morphology.

Spectral types can be obtained through high S/N spectra, or through fitting of the spectral energy distributions of the galaxies. The approach that we use in this paper is to fit spectral energy distributions to the broad-band photometry of our sources and to derive which is the best fitting spectral type - elliptical, early-type spirals, late-type spirals, irregulars and starbursts (§3.4). This is similar to our morphological scheme in principle, although there is no reason why these spectral-types should match morphological ones at $1 < z < 3$ as well as they do at lower redshifts.

First, we give some numbers on the overlap of these types. At $1 < z < 2$, we find that for systems identified as disk galaxies and edge-on disk galaxies visually, 86% (83%) of systems have a spectral-type consistent with a disk, i.e., Sbc/Scd types (where the second number is parenthesis is the edge-on disk fraction). For the remainder, we find that 7% (17%) of disks have an early-type spectral-type, and 7% (0%) have spectral types that are star forming/starbursts. What this shows is that our visual estimates are roughly correct in identifying which systems have a mix of stellar populations - i.e., a mixture of an old and a younger component. At higher redshifts ($2 < z < 3$) we find for both types of disks that 100% are identified as Sbc/Scd spectral types.

For systems identified as visual early-types in WFC3 imaging, we find a more mixed outcome. At $1 < z < 2$ we find that only 10% of these systems would be identified as E-spectral types. That is, only a very small fraction of the WFC3 imaged UDF galaxies we find visually as early-types have a spectral shape suggesting that they contain evolved stellar populations. The bulk of the visually classified early-types are found to be consistent with a Sbc/Scd spectra type (56%) at $1 < z < 2$, suggesting a mixture of old+young stel-

lar populations, or the fading of an older stellar population that did not form in one complete burst. Interestingly, 34% of the visually classified early-types at $1 < z < 2$ are consistent with being starbursts or Im systems - that is galaxies which are dominated by star formation. This rises to 62% starburst spectral-types for visually classified early-types at $2 < z < 3$. We will return to a discussion of this issue in §5 and what it implies for early-type formation.

The two final visual categories we discuss are the peculiars and the peculiar early-types, which are systems that resemble early-types in some formation state and display a visual peculiarity. What we find is that at the higher redshift range, $2 < z < 3$, these two types have similar spectral energy distributions - the visually classified peculiars are 62% starburst/Im spectral type, and 38% Sbc/Scd type. Very interestingly, this is just slightly less than the fraction of visually classified early-types which are star forming. As for the peculiar early-types, we find a very similar fraction of 60% Im/starburst spectral-type and 40% Sbc/Scd. Based on this, it appears that the peculiar/E/pE types may have a similar origin, and this is reflected in the similar spectral types of all these types.

At lower redshifts, $1 < z < 2$, we find that the fraction of peculiars which remain starburst/Im systems drops to 35%, with 10% having an E spectral type, and 55% having a Sbc/Scd spectral type. This is very similar to the breakdown for the ellipticals. This shows that peculiar galaxies are not all starbursting systems, but likely are distorted due to perhaps the merging of existing galaxies which contain a mixture of old and young stellar populations. The peculiar ellipticals at $1 < z < 2$ are 53% starburst/Im spectral types and 47% Sbc/Scd spectral types, showing a similar pattern to the peculiars, but with even more systems having a starburst origin.

4.6 Tracing Galaxy Formation and Actual Types

There are two goals to studying galaxies in terms of their structure in this paper. These are understanding when and how the Hubble sequence was put into place. Clearly, as we have just shown, the Hubble sequence, as we know it today, does not exist at higher redshifts, particularly at $z > 2$. The question becomes - how can we identify galaxies at higher redshifts that match the properties of nearby Hubble types? This goes beyond morphology and asks the question - when do ellipticals, in the sense of smooth, nearly structureless galaxies dominated by old stellar populations, first form? Related to this is the formation of galaxies with disks. The former problem of the ellipticals is easier to probe, in principle, as finding a galaxy with a smooth morphology and older stellar populations is more straightforward than determining if a galaxy is a rotating disk. We also investigate whether we can use structure to determine the formation modes of galaxies, where we consider the merger history in §4.6.3.

4.6.1 A ‘Pure’ Elliptical Evolution

First, we discuss the fraction of pure ellipticals within the UDF. We define pure ellipticals as galaxies which have a spectral-type consistent with an early-type, and a morphology consistent with being a modern elliptical, which we se-

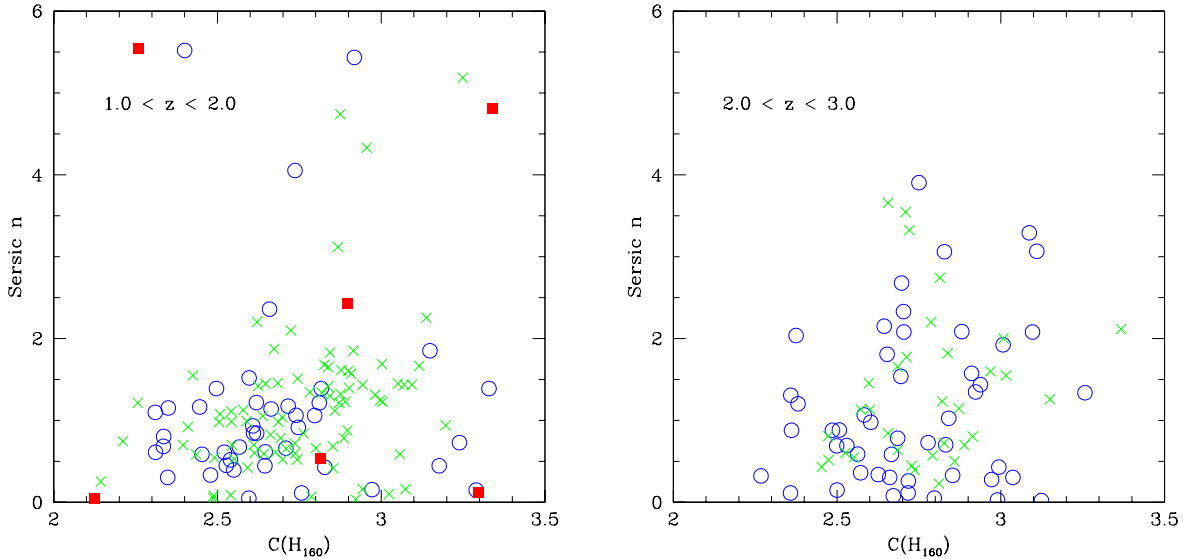


Figure 14. Plot showing the relationship between the concentration parameter C and the Sérsic index, n for galaxies divided into redshift ranges $1 < z < 2$ and $2 < z < 3$. Shown on this panel as well are the spectral classification types, with the following labelling scheme: the solid red open boxes are classified as early-type spectrally, open blue circles are starforming systems, the Im/starbursts, and the green crosses are those classified spectrally as disk like, or Sbc/Scd.

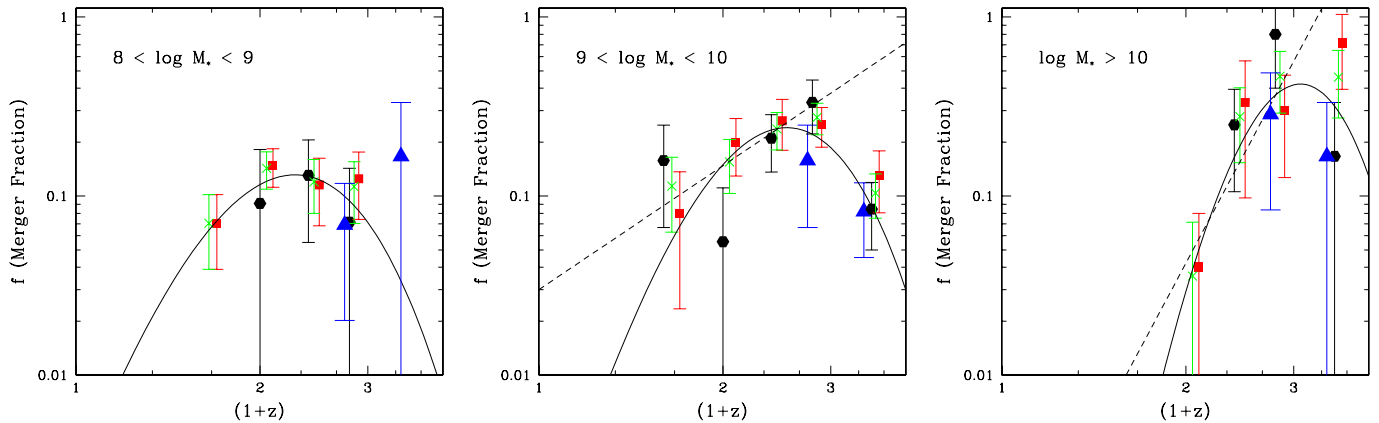


Figure 15. The merger fraction as a function of redshift and stellar mass for our WFC3 sample (blue triangles) compared with data from the Hubble-Deep Field North NICMOS (red squares) and the ACS Ultra-Deep Field (black circles). Shown in this figure are the merger fractions at mass limits of $8 < \log M_* < 9$, $9 < \log M_* < 10$, and $\log M_* > 10$. The green crosses show the evolution of the merger fraction for a combined UDF and HDF-N sample.

lect as $A < 0.2$. At $z = 0$ the elliptical fraction for galaxies with stellar masses $M_* > 10^{10} M_\odot$ is $> 20\%$ (Conselice 2006a). With our selection, we find a much smaller fraction at higher redshifts.

When we examine the evolution of this pure elliptical fraction with redshift we find that there are no pure early-type at $z > 2$. We find a total of six systems at $1 < z < 2$

giving a fraction of $3.2 \pm 2.3\%$ at $1.5 < z < 2.0$ and $4 \pm 2\%$ at $1 < z < 1.5$. We find a higher fraction if we limit our selection to $M_* > 10^{10} M_\odot$ systems = $14 \pm 14\%$ at $1.5 < z < 2$ and $23 \pm 13\%$ at $1 < z < 1.5$. This demonstrates that massive galaxies are more likely to be elliptical than lower mass ones, which is also seen in the nearby universe (e.g., Conselice 2006a). This also shows that at least within the very

small field of view of the UDF, there are no pure elliptical galaxies at $z > 2$. However, most certainly progenitors of pure ellipticals exist at these redshifts, and the fact that there are massive galaxies, even within our own sample, at $z > 2$ shows that these galaxies are in an active assembly mode, and can be identified and studied. Future studies of larger fields, especially within the CANDELS programme, will address these issues, and put better constraints on the number of passive ellipticals at $z > 2$

4.6.2 *The Disk Galaxies*

Tracing disk galaxies in a similar way as the ellipticals is not as straightforward. However, the disk galaxies at the magnitude and stellar mass limits we use are extremely common in the nearby universe, with a fraction of 60-75%. Thus, just from this, a significant number of the distant galaxies we see must be progenitors, in some form, of disk galaxies in today's universe. The issue with disks is that the spectral-type is a mixed population of older and younger stars, which is not an unusual situation at high redshift, and does not necessarily imply that these systems are always disks - consisting of an older bulge with a younger disk. Structurally disks can be identified by having a modest asymmetry and concentration. When we examine systems within our sample with $C < 3$ and $0.2 < A < 0.35$, and spectral types consistent with nearby disks, we find a roughly even fraction of disks of 7-15% between redshifts of $1 < z < 3$, which is similar to the visual fraction (Figure 5).

However, when we use these limits we find that the galaxies we select are not always identifiable as disks visually, in fact they often are not. We in fact classify most of these systems as peculiars or compact galaxies, showing that the apparent morphology of galaxies can be quite different from what their structure and stellar populations are revealing.

An alternative method for understanding the limits of the number of disks we have is by examining the fraction of systems with large inclinations, which are likely disks seen edge-on. Through the use of our measured ellipticities with GALFIT, we find that roughly 30% of our selected systems have an axis ratio $b/a < 0.3$. If all of these are edge on systems, then every galaxy at these redshifts from $z = 1 - 3$ would have to be a 'disk' galaxies. While this is obviously unlikely the case, it shows that we are likely misidentifying some disks, although many of these disks are likely in some formation mode and cannot be identified as such. This issue was furthermore examined recently for massive compact quiescent galaxies at $z \sim 2$ by van der Wel et al. (2011) who found that $65 \pm 15\%$ of massive compact systems are likely disks in some form. While it is unlikely that every galaxies in our sample is a disk in some form, it does show that we are very likely under representing the number of disk galaxies in our sample by using either visual morphologies or parametric parameters (see also Buitrago et al. 2011, in prep).

4.6.3 *The Merger History*

In this section we revisit the measurement of the merger history which was used in Conselice et al. (2008) with ACS

UDF data, and Conselice et al. (2003) using NICMOS imaging of the HDF-N to trace the merger history for galaxies as a function of stellar mass at $z > 1$. Both of these studies found similar results, that the merger history is highest for the most massive galaxies at $z \sim 2.5$, and declines steeply at lower redshifts, while lower mass systems have a more gradual drop off in their merger fraction. Conselice et al. (2008) and Conselice (2006b) investigate, using these merger fractions, the likely merger rate, and the contribution of merging to building up the stellar masses of galaxies over time.

We use WFC3 data from this paper to make a new measurement of the merger history with WFC3 data at $z > 1$, and compare this with previous work. The errors on these measurements are large simply because of the small number of galaxies used in this study. Future work using data such as CANDELS will address the merger history issue in much more detail. For now however, we simply describe the merger history, and how it agrees with previous results.

First we describe our measured merger fractions based on the CAS parameters. This is a topic with a large history and background, but the most relevant papers for measuring the merger history with CAS are Conselice (2003), Conselice et al. (2003), Conselice et al. (2008) and Conselice, Yang & Bluck (2009). As described in Conselice et al. (2000a,b) and Conselice (2003) one method for finding mergers is to use the conditions in rest-frame optical light (cf. Taylor et al. 2007; Lanyon-Foster et al. 2011 for UV),

$$A > 0.35 \ \& \ A > S, \quad (5)$$

such that the asymmetry is higher than $A = 0.35$, and the asymmetry value is higher than the clumpiness value, $A > S$. This ensures not only that a galaxy is roughly 1/3 asymmetric in terms of its light distribution, but also that this light does not come from clumpy light, such as star forming regions. This method works well at lower redshifts (Conselice 2003), yet with the larger star forming clumps seen within high- z galaxies (e.g., Elmegreen et al. 2005) it remains possible that some galaxies with large star forming complexes are being misidentified as a merger.

We show the merger fraction using our new WFC3 UDF imaging in Figure 15, finding a very similar merger fraction as before using ACS. One way to quantify this merger history is through various fits of the merger fraction history. The traditional power-law format (Conselice et al. 2003a,b; Bridge et al. 2007; Conselice et al. 2009; Bluck et al. 2009) is given by:

$$f_m(z) = f_0 \times (1 + z)^m \quad (6)$$

where $f_m(z)$ is the merger fraction at a given redshift, f_0 is the merger fraction at $z = 0$, and m is the power-law index for characterising the merger fraction evolution. An alternative way to characterise the merger fraction evolution is the Press-Schechter formalism (Conselice et al. 2008) - which is essentially a combined power-law+exponential form. However, we do not consider this form in this paper, but will in future investigations of the merger history.

By fitting equation 6, we find a similar parameterisation of the merger history as we found for galaxies with an m exponent of $m \sim 5.5$, for massive galaxies and $m \sim 2.2$ for lower mass systems. We also show on Figure 15 the best fitting exponential/power-law form for the merger history. Integrating the merger rate, using a time-scale of 0.4 Gyr

(Conselice et al. 2008) we find that on average there are $4.3_{-0.8}^{+0.8}$ major mergers at $z < 3$ for the most massive galaxies with $M_* > 10^{11} M_\odot$. This is enough merging to roughly double the mass of these galaxies (Conselice 2006b). In the future, we will be utilising more wide-field imaging from CANDELS and other WFC3 surveys to obtain a more accurate and definite merger history for these galaxies.

4.7 Comparison to Models

In this section we carry out a comparison between our results, and models of galaxy formation which can predict the evolution of galaxy morphology as a function of redshift. The models we compare with are the *Galacticus* semi-analytical models from Benson & Devereux (2010) and Benson (2010) which do not resolve the morphologies of galaxies as some numerical models do. However, these models follow the formation of galaxies in a cosmological context, and can be used to predict how spirals, ellipticals and galaxy mergers evolve through time based on the physics which is thought to form these systems.¹

Currently, the idea is that galaxies are formed from mergers and accretion. Bulges and ellipticals are formed in merger events that have dynamically cooled and relaxed, while disks and spirals are formed by the smooth accretion of intergalactic gas which is then converted into stars over some time period. These models predict these quantities, as well as the time since the last major merger for each galaxy at a given redshift.

We use these models to predict the morphological evolution of galaxies in a cosmological context, and therefore whose formation is influenced by the relative distribution of dark matter, dark energy and the temperature of the dark matter. These models are such that a measure of the bulge to total ratio can be derived based on the history of spheroidal and disk assembly. Thus, while these models do not resolve galaxy morphology, they can predict what the likely morphological distribution is based on the physics of the galaxy formation.

This comparison is shown in Figure 16 between our three main types and the same predictions from Benson & Devereux (2010). The way to view this comparison is that the data has the same line type as in Figure 16, and the predictions of the same quantities are shown as double lines. The green doubled dashed line shows the evolution of the disk fraction, as defined by $B/T < 0.5$. The red short dashed line shows predictions for the evolution of the elliptical fraction, as defined by $B/T > 0.9$. The merger fraction predicted in the simulation are galaxies defined as having had a major merger in the past 1 Gyr, similar to what would be predicted for producing a peculiar galaxy (Conselice 2006b).

The comparison between these quantities is fairly good using these definitions, which are somewhat arbitrary as we do not know, nor have an obvious way, to compare which B/T ratios correlate with early/late type disks. This is demonstrated by the white dot-dashed, which is the fraction of systems with $0.5 < B/T < 0.9$, which ranges from a fraction of roughly 0.4 to 0.6 within our range of interest. If we consider these systems are ‘early-type’, or based on the

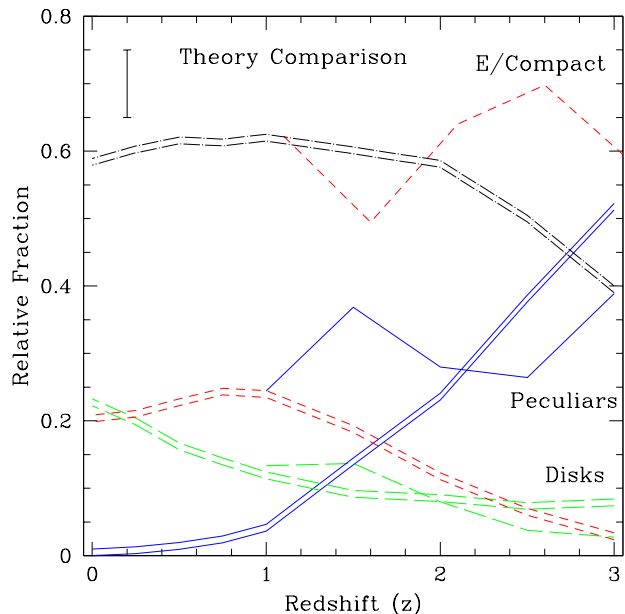


Figure 16. The comparison of our WFC3 morphologies, probing the rest-frame optical at $1 < z < 3$ and model predictions from Benson & Devereux (2010). The single lines are the data, as shown in Figure 5, where the dashed line red line is the E/Compact systems, the solid blue line denote the peculiar systems and the dashed green line is for those galaxies classified as disks. The double dashed lines, with the same colour and line type as the data, are the model predicts from Benson & Devereux (2010). In the models the E/Compact is for systems with $B/T > 0.9$, and the disks are systems with $B/T < 0.5$, and the peculiars are systems which have undergone a merger in the past Gyr. The black dot-dashed line shows the fraction of systems with $0.5 < B/T < 0.9$.

results in §4.3 as indeed true disks which appear as early-types in our classification due to the effects of redshift, then the predicted fraction would agree quite well with the early-type fraction we observe. However, previous work on more detailed comparisons between mergers and theory predictions show a worse agreement (Bertone & Conselice 2009).

5 SUMMARY

This paper presents an analysis of galaxy morphology and structure at $1 < z < 3$ using WFC3 data utilising several popular approaches, include visual estimates of morphology, CAS parameters, parametric Sérsic profile fitting, as well as spectral-type fitting to spectral energy distributions. We furthermore analyse morphological k -corrections between ACS and WFC3, essentially probing the difference in rest-frame morphology between the ultra-violet and optical light at $z > 1$. Our major findings include:

I. In terms of morphological k -corrections, a large fraction of systems classified as ‘peculiar’ at $1 < z < 3$ within

¹ The exact model we use is version 0.9.0.r249 of Galacticus.

ACS imaging appear as early-types in the WFC3 imaging. This result holds to some degree even after convolving the ACS image with the larger WFC3 PSF, and by simulating nearby galaxies to high- z , and redoing classifications. However, these ‘early-types’ are clearly not the same as those at $z = 0$ in terms of their stellar populations, showing evidence for star formation and ongoing assembly.

II. We further find that these ‘early-type’ classifications dominate the non-peculiar galaxy population at $1 < z < 3$, with a fraction near 30%, with a similar fraction of peculiars. The remaining systems are classified as ‘compact’ galaxies, and disk-like galaxies, which are both on average 10-20% of the population.

III. We show that there is a significant difference in the population of galaxies classified as early/mid/late types as defined by spectral-types and those defined through visual estimates. The most common difference is found for galaxies classified as elliptical – a significant fraction of these have a disk spectral type, or even a starburst spectral type. This shows that very few purely passive massive galaxy exist at $1 < z < 3$, at least within the UDF.

IV. Examining the CAS parameters, we find that the change in CAS values between the z_{850} and H_{160} bands is similar, per unit wavelength, as found between the rest-frame UV and optical at $z < 1$ (Conselice et al. 2008).

V. By using a strict definition of elliptical and disk galaxies that matches the concentration, asymmetry, and spectral types for nearby systems, we find very few ‘formed’ systems at $z > 1$. We find 10% of our sample would be classified as nearby disks at $z > 1$, compared with 75% in the modern universe. Likewise, we find $< 5\%$ of systems classifiable as modern ellipticals, about a factor of three lower than today.

VI. We find that the inferred merger fraction for the most massive galaxies ($> 10^{10} M_{\odot}$) at $z > 1$ is between 20-30%. This is very similar to previous findings using UDF ACS and NICMOS HDF imaging, revealing that even when probing the rest-frame optical at $z > 1$ we find a similar merger history, and therefore a similar contribution of mergers towards forming galaxies, as when looking at lower resolution and bluer wavelengths.

VII. We find that the properties of visually classified elliptical peculiars, and the peculiar ellipticals are very similar, suggesting that these galaxies are in some common formation scenario. It is very likely that this common process is galaxy merging, with each type in a different phase of merging. We are therefore likely seeing the formation modes of elliptical galaxies through these systems.

We do not find a large fraction of visually classified disk galaxies at $z > 1$ (10-15%). This is potentially due to misidentifying ellipticals as rotating disks, however the spiral structure, and star forming regions seen in disks at $z < 1$ and at times at $z > 1$ should be visible within our imaging. The number of edge-on disk galaxies, and the high number of inclined systems we see, suggests that perhaps we are misidentifying some face-on disks as ellipticals, however, the mode of formation of these systems must be quite different from spirals in the more nearby universe.

Overall, our conclusion is that visual estimates of morphology are limited, both because of the PSF of WFC3 limits our ability to resolve distant galaxies, as well as the intrinsic nature of morphology at higher redshifts. We demonstrate that the best way to find distant galaxy ‘type’ analogs to modern galaxies, and therefore to address the question of how and when the Hubble sequence forms is through quantitative measurements of both the stellar populations and quantitative structures, and leaving behind visual estimates.

We acknowledge support for this work from STFC in the form of post-doctoral research assistant and studentship support, and the Leverhulme Foundation in the form of a Leverhulme Trust Prize to CJC. We thank Andrew Benson for providing us with the latest output of his Galacticus semi-analytical model.

REFERENCES

- Abraham, R.G., Tanvir, N.R., Santiago, B.X., Ellis, R.S., Glazebrook, K., van den Bergh, S. 1996, MNRAS, 279, 47L
- Benitez, N. 2000, ApJ, 536, 571
- Beckwith, S., et al. 2006, AJ, 132, 1729
- Bershady, M.A., Jangren, J.A., Conselice, C.J. 2000, AJ, 119, 2645
- Bertone, S., Conselice, C.J. 2009, MNRAS, 396, 2345
- Bluck, A.F.L., Conselice, C.J., Bouwens, R.J., Daddi, E., Dickinson, M., Papovich, C., Yan, H. 2009, MNRAS, 394, 51L
- Bouwens, R.J., et al. 2009, ApJ, 705, 936
- Bridge, C., et al. 2007, ApJ, 659, 931
- Buitrago, F., Trujillo, I., Conselice, C.J., Bouwens, R.J., Dickinson, M., Yan, H. 2008, ApJ, 687, 61L
- Cameron, E., et al. 2010, arXiv:1007.2422
- Cassata, P., et al. 2005, MNRAS, 357, 903
- Cassata, P., et al. 2010, ApJ, 714, 79L
- Coe, D., Benitez, N., Sanchez, S.F., Jee, M., Bouwens, R., Ford, H. 2006, AJ, 132, 926
- Coleman, G. D., Wu, C.-C., Weedman, D. W. 1980, ApJS, 43, 393
- Conselice, C.J. 1997, PASP, 109, 1251
- Conselice, C.J., Bershady, M.A., Jangren, A. 2000a, ApJ, 529, 886
- Conselice, C.J., Bershady, M.A., Gallagher, J.S. 2000b, A&A, 354, 21L
- Conselice, C.J. 2003, ApJS, 147, 1
- Conselice, C.J., Bershady, M.A., Dickinson, M., Papovich, C. 2003a, AJ, 126, 1183
- Conselice, C.J., Chapman, S.C., Windhorst, R.A. 2003b, ApJ, 596, 5L
- Conselice, C.J., Gallagher, J.S., Wyse, R.F.G. 2002, AJ, 123, 2246
- Conselice, C.J., Blackburne, J., Papovich, C. 2005, ApJ, 620, 564
- Conselice, C.J. 2006a, MNRAS, 373, 1389
- Conselice, C.J. 2006b, ApJ, 638, 686
- Conselice, C.J., Rajgor, S., Myers, R. 2008, MNRAS, 386, 909
- Conselice, C.J., Yang, C., Bluck, A.F.L. 2009, MNRAS, 394, 1956
- Conselice, C.J., et al. 2011, MNRAS, in press, arXiv:1010.1164

- Dahlen, T. et al. 2010, ApJ, 724, 425
Dekel, A. et al. 2009, Nature, 457, 451
Dickinson, M., et al. 2000, ApJ, 531, 624
Driver, S.P., Windhorst, R.A., Ostrander, E.J., Keel, W.C.,
Griffiths, R.E., Ratnatunga, K.U. 1995, ApJ, 449, 23L
Elmegreen, D.M., Elmegreen, B.G., Rubin, D.S., Schaffer,
M.A. 2005, ApJ, 631, 85
Genzel, R., et al. 2006, Nature, 442, 786
Giavalisco, M., Livio, M., Bohlin, R.C., Macchetto, F.D.,
Stecher, T.P. 1996, ApJ, 112, 369
Giavalisco, M., et al. 2004, ApJ, 600, 93L
Grogin, N.A., et al. 2005, ApJ, 627, 97L
Hernandez-Toledo, H.M., Avila-Reese, V., Conselice, C.J.,
Puerari, I. AJ, 2005, AJ, 129, 682
Hopkins, P., Hernquist, L., Cox, T.J., Di Matteo, T.,
Robertson, B., Springer, V. 2006, ApJS, 163, 1
Kinney, A.L., Calzetti, D., Bohlin, R.S., McQuade, K.,
Storchi-Bergmann, T., & Schmitt, H.R. 1996, ApJ, 467,
38
Lotz, J.M., Primack, J., Madau, P. 2004, AJ, 128, 163L
Overzier, R.A., Heckman, T.M., Schiminovich, D., Basu-
Zych, A., Goncalves, T., Martin, D.C., Rich, R.M. 2010,
ApJ, 710, 979
Peng, C., Ho, L.C., Impey, C.D., Rix, H.-W. 2002, AJ, 124,
266
Ravindranath, S., et al. 2006, ApJ, 652, 963
Roberts, M.S., Haynes, M.P. 1994, ARA&A, 32, 115
Shapiro, K.L., et al. 2008, ApJ, 682, 231
Taylor-Mager, V., Conselice, C., Windhorst, R., Jansen, R.
2007, ApJ, 659, 162
Thompson, R.I. et al. 2005, AJ, 130, 1
Trujillo, I., Conselice, C.J., Bundy, K., Cooper, M.C.,
Eisenhardt, P., Ellis, R.S. 2007, MNRAS, 382, 109
van der Wel, A., et al. 2011, ApJ, 730, 38